AFFDL-TR-71-181

A STUDY OF THE BLUNT SLAB DELTA WING AT HYPERSONIC SPEEDS AND ANGLES OF ATTACK

GERALD L. BURKE

FOREWORD

This report was written by G. L. Burke of the High Speed Aero Performance Branch, Flight Mechanics Division, Air Force Flight Dynamics Laboratory, Wright-Patterson Air Force Base, Ohio. The work was accomplished under Project 1366, "Aeromechanics Technology for Military Aerospace Vehicles" Task 136607, "High Speed Aerodynamic Heating to Military Flight Vehicles". The report presents exploratory development conducted under Work Unit 136607 003, "Heat Transfer Design Criteria for High Speed Military Systems".

The report covers data taken during wind tunnel experiments conducted between August 1964 and September 1969. The report was written between September 1969 and September 1970. The report was submitted for review in January 1971.

The author wishes to acknowledge the assistance of Brian Van Vliet, engineering co-op, who did the data reduction and graphical analysis.

This technical report has been reviewed and is approved.

Alfred C. Draper

for PHILIP P. ANTONATOS
Chief, Flight Mechanics Division
Air Force Flight Dynamics Laboratory

ABSTRACT

This report presents information obtained during an extensive AFFDL study of the flow field about blunt, slab delta wings. Data taken during the study include surface heat transfer and pressure, pitot surveys, oil flows, schlierens, shadowgraphs, and vapor screens.

The main lesson of the study is the three-dimensionality of the flow field in addition to the documented effects of inflow and outflow. The most unexpected phenomenon was the appearance of a hot streak on the lower surface off the center line. It is proposed that this region of higher heating is due to a slip line originating at the point of inflection in the shock wave between the bow shock and the leading edge shock. This proposition is supported by pitot pressure surveys and surface pressure distributions.

Other qualitiative features of the flow field which are presented include the movement of the leading edge stagnation line onto the lower surface. The relative entropy levels of the flow field and the use of vapor screens in hypersonic tunnels are discussed.

TABLE OF CONTENTS

ILLUSTRATIONS

ILLUSTRATIONS (Contd)

LIST OF SYMBOLS

B.L.	Boundary layer
BS	Body station, measured from nose tip in plan view
D	Diameter of nose or leading edge (in.)
h	Heat transfer coefficient (BTU/ft^2-sec- R)
L	Distance along leading edge measured from apex of slab portion of wing (in.)
M	Mach number
P	Pressure (psia)
P_o'	Pitot pressure in free stream of wind tunnel
P_T	Measured pitot pressure in model local flow field
S_t	Stanton number
R	Radius of nose or leading edge (in.)
R_e	Reynolds number
X	Distance parallel to center line measured from leading edge in plan view (in.) (Figures 1 and 2)
Y	Distance normal to model surface measured from surface (in.)
Z	Distance from model center line measured along surface from the center line (in.) (Figures 1 and 2)
α	Angle of attack (degrees)
θ	Local shock wave inclination angle measured with respect to free stream (degrees)
θ^*	Value of θ with aft shock Mach number of unity
Subscripts	
D	Experimental data value
S	Conditions at shock wave
T	Based on theoretical calculations
∞	Conditions in wind tunnel free stream

SECTION I

INTRODUCTION

The blunt slab delta wing has been under investigation as a candidate lifting reentry configuration since the X-20 program. Basic aspects of the flow field were identified and correlated as early as 1960 by Bertram, et al in Reference 1 using the still current method of strip theory, stream line divergence theory, and cross flow theory. These theories, which were developed during the parametric design study of the X-20 program, are described in Reference 2. The ASSET, even though it was a blunt configuration, was designed using the strip and stream line divergence theories (Reference 3). Very little correlation of inflow effects on blunt leading edge configurations (which thickens the boundary layer on the center line and decreases heating rates to less than strip theory values) has been attempted.

The Air Force Flight Dynamics Laboratory has continued the delta wing exploratory development program since ASSET in support of the proposed high lift-to-drag ratio reentry system and, currently, in support of the space shuttle. Reports on these tests are listed as References 3 to 26.

Historically, delta wing lower surface heat transfer data have been correlated by plotting some heating term as a function of length for the model center line. It is along this line of symmetry for which the stream line divergence and cross flow theories were derived. However, the critical heating design point on the lower surface is not on the center line but along the juncture line of the lower surface and leading edge materials. At a point along this line, two materials with different thermal capacities are subjected to the same heating rate and it must be insured that the "weaker" material is not over-stressed. In order to allow for this, the designer must have information on magnitudes and gradients in the region between the center line and leading edge. It was with this goal in mind that AFFDL began concentrating on off center line measurements of heat transfer, pressure, and pitot pressure surveys.

Particular interest in off center line measurements was generated after a series of vapor screen tests on the ASSET configuration which revealed strange patterns in the "boundary layer" growth. Following this, vapor screen tests were conducted on sharp and blunt slab delta wings at Mach 10. Comments on these tests are made in Section III. The second part of Section III discusses pitot pressure surveys and briefly introduces oil flows at a convenient point. The third part presents surface heat transfer and pressure measurements.

Many data points have been generated during the study reported herein. However, no attempt will be made to correlate the data or to generate heat transfer design techniques. Instead, this report will emphasize some of the basic features of the flow which must be taken into account when formulating flow models to use in correlations.

SECTION II

TEST DESCRIPTION

A total of five different models were used during this investigation. Two of these were 70° sweep delta wings with .25-inch nose and leading edge radii. Model 1 was 12 inches long and was instrumented with thermocouples for measuring heating rates at Mach 6, 8, and 10. Model 2 was 18 inches long and was used for flow field studies including shadowgraphs and schlierens, oil flow, vapor screens, and pitot pressure surveys at Mach 10. These models are shown in Figure 1.

Model 3 was a 75° sweep, 34 inch-long delta wing with sharp nose and leading edges. The model was uninstrumented and only oil flow, vapor screens, and schlierens were taken at Mach 10.

The last two models were both 80° sweep, 30-inch long delta wings with .5-inch nose and leading edge radii. Model 4 was instrumented with thermocouples and was tested at Mach 6, 8, and 10. Model 5 was instrumented with surface pressure taps and was also used to obtain oil flow, shadowgraph, schlieren, vapor screen, and pitot survey data at Mach 8 and 10. This last model was later modified by grinding the nose and leading edge down to a .25-inch radius. These models are shown in Figure 2.

All experiments were conducted at the Arnold Engineering Development Center in Tunnels B and C of the von Karman Facility. These tunnels are described in the Test Facilities Handbook, Reference 27. A summary of model dimensions and test conditions is given in Table I.

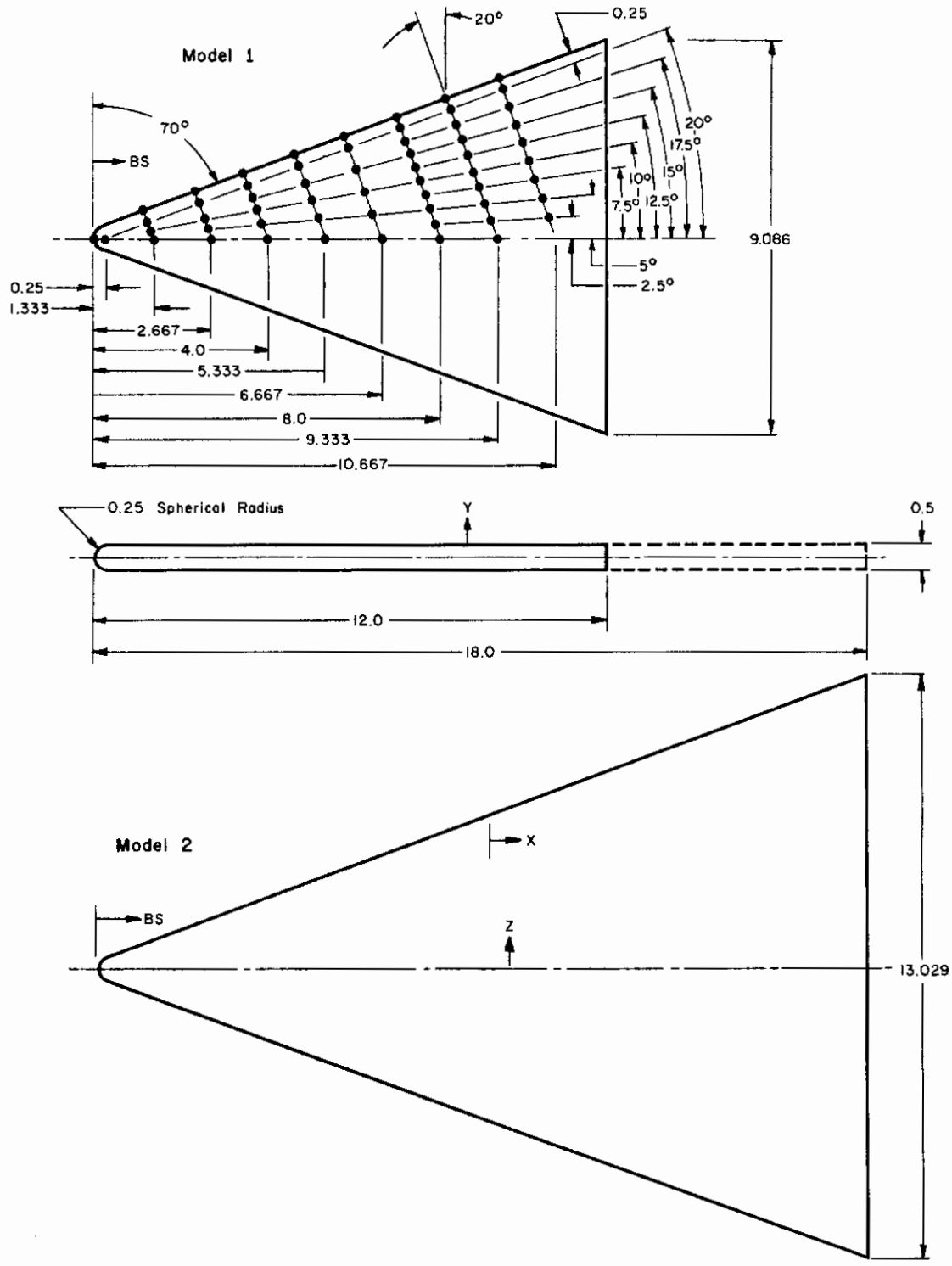

Figure 1. 70° Swept Delta Wings

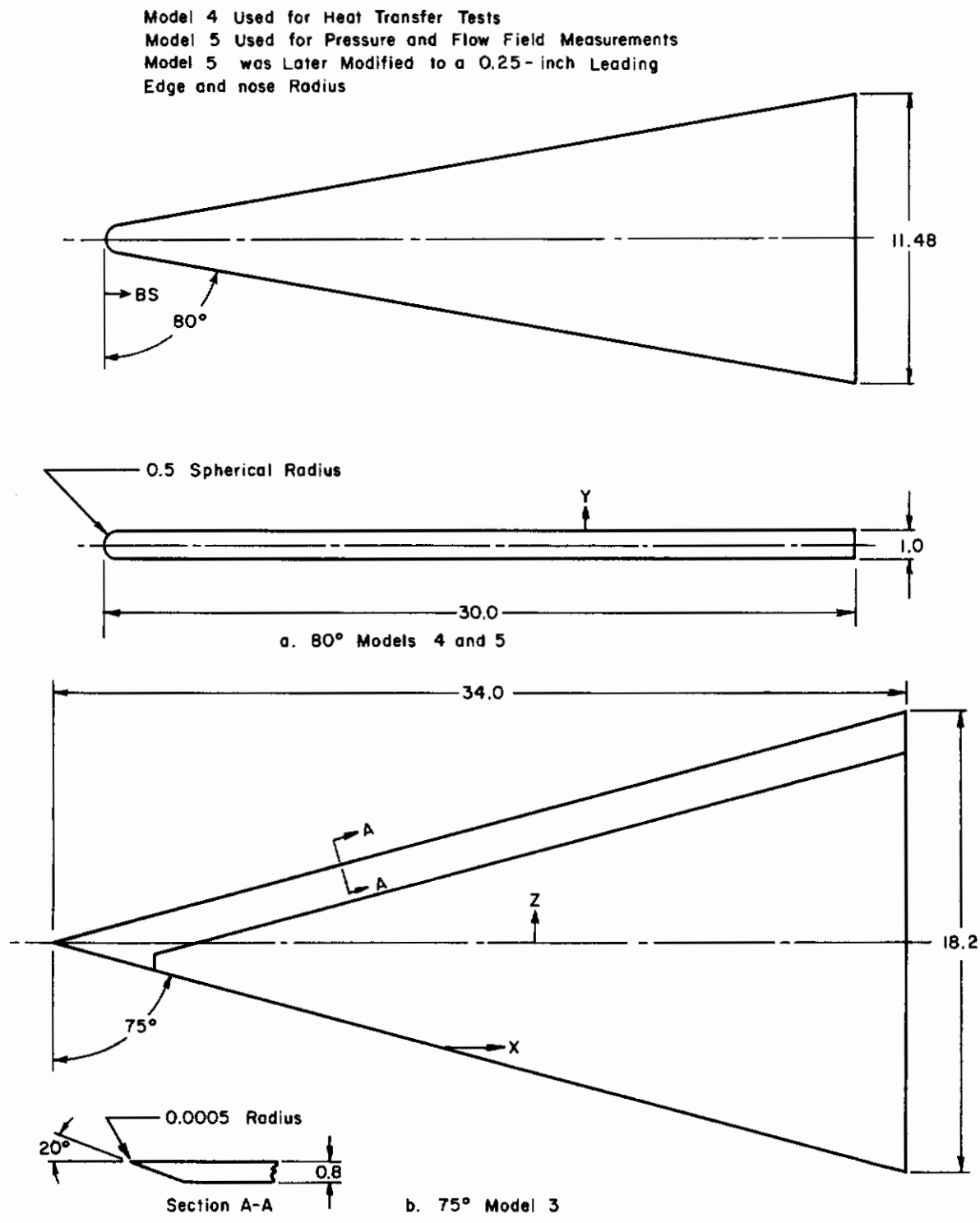

Figure 2. 75 and 80° Delta Wings

TABLE I

MODEL INFORMATION

Model	Sweep	Radii	Length	Instrumentation	Measurements	M_∞
1	70	.25	12	Thermocouples	Heating rates	6, 8, 10
2	70	.25	18	None	Pitot pressure surveys vapor screens oil flow shadowgraphs schlierens	10
3	75	zero	34	None	Oil flow vapor screens schlierens	10
4	80	.50	30	Thermocouples	Heat transfer	6, 8, 10
5	80	.50 (.25)	30	Surface pressure	Pressure pitot survey vapor screen oil flow shadowgraph schlieren	8, 10

SECTION III

DISCUSSION

1. VAPOR SCREEN STUDIES

Vapor screens are produced by operating the wind tunnel at a lower total temperature than normal (T_o = 750°R rather than 1800 for Mach 10) so that the air condenses upon expansion into the test section. The flow is illuminated by a high intensity light source (laser) operating through a slit which produces a white screen due to condensed particles dispersing the light. Any disturbance in the stream, such as a boundary layer, shock wave or vortex on a model surface, changes the uniform distribution of condensed particles resulting in relatively lighter and darker patterns. A reduction in the number density of particles results in a darker region while an increase would raise the intensity of reflected light.

One of the first questions to be answered when using vapor screens is the effect of condensation on flow properties. In order to possibly determine this effect, schlieren photographs and pitot pressure surveys were made during liquified conditions for comparisons with similar measurements under normal test conditions.

Measurements of the difference of the shock displacement along the 18-inch blunt 70° Model 2 center line due to liquefied flow are shown in Figure 3. The only consistent difference which could be attributed to condensation occurs at the lower angles of attack (0 and 4°) and at body station 12 and greater. The effect on pitot pressure surveys was more drastic as seen in Figures 4 and 5 where the difference in magnitude and gradients is obvious, particularly at angles of attack less than five degrees. However, at angles of attack of 8 and 12 degrees, the gradient and magnitude are approximately equal near the model surface. Also, in the condensed flow case, a constant aft-shock pitot pressure is not attained for angles at which a near constant value is reached under standard operating conditions. These figures also show the reduction in free stream pitot pressure during condensed flow. This is consistent with the lower total temperature, higher Reynolds number, thinner tunnel wall boundary layer, and higher free stream Mach number.

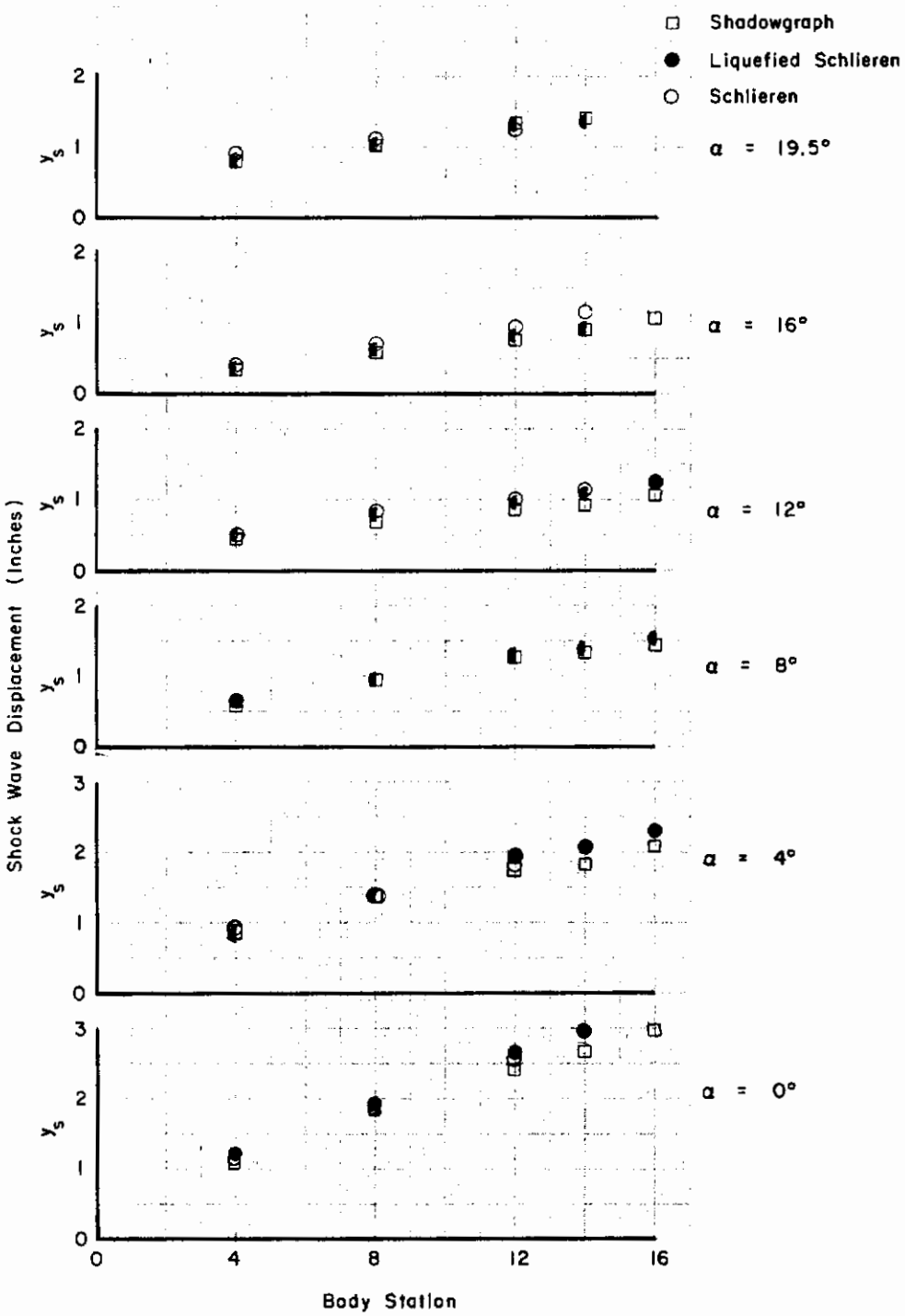

Figure 3. Effect of Flow Condensation on Shock Wave Displacement on Model 2 at Mach 10

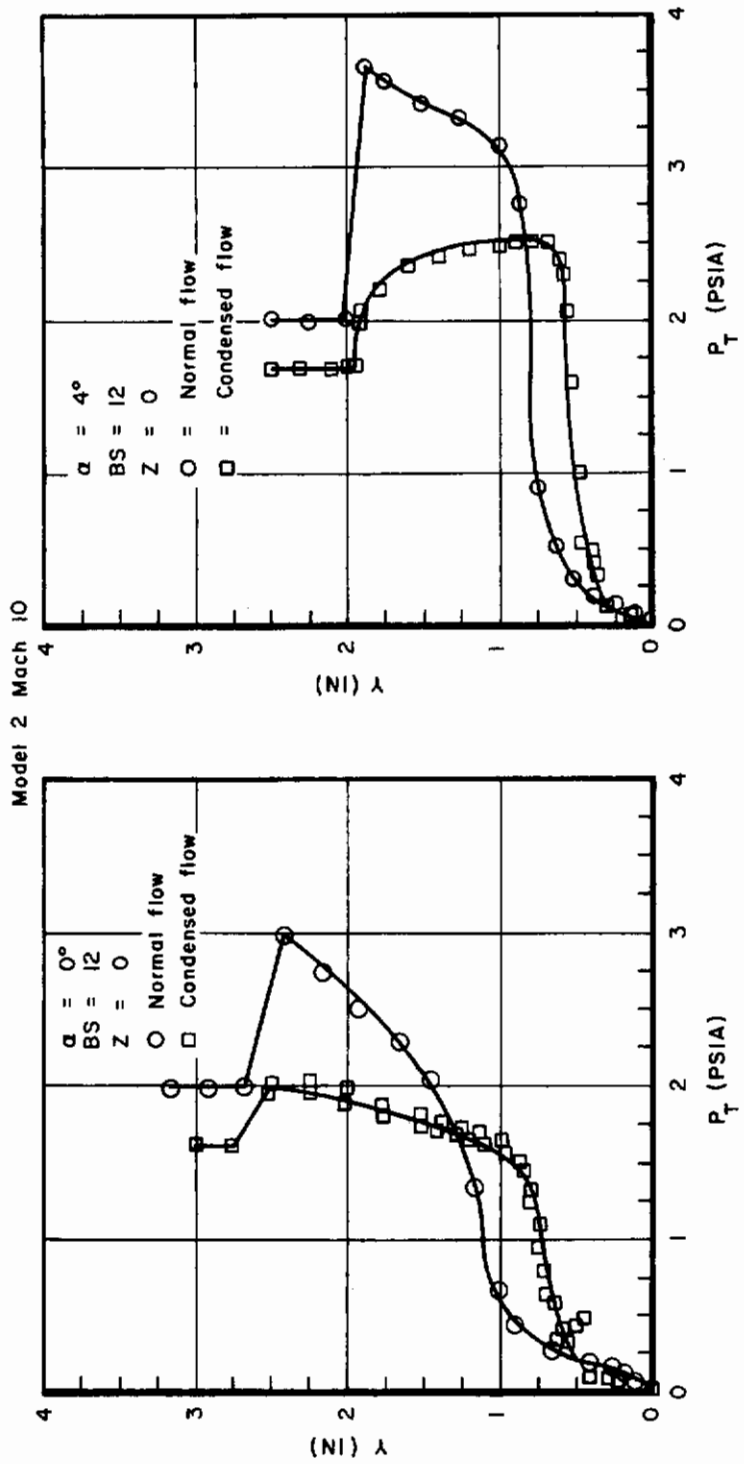

Figure 4. Effects of Condensed Flow on Pitot Pressure Profiles

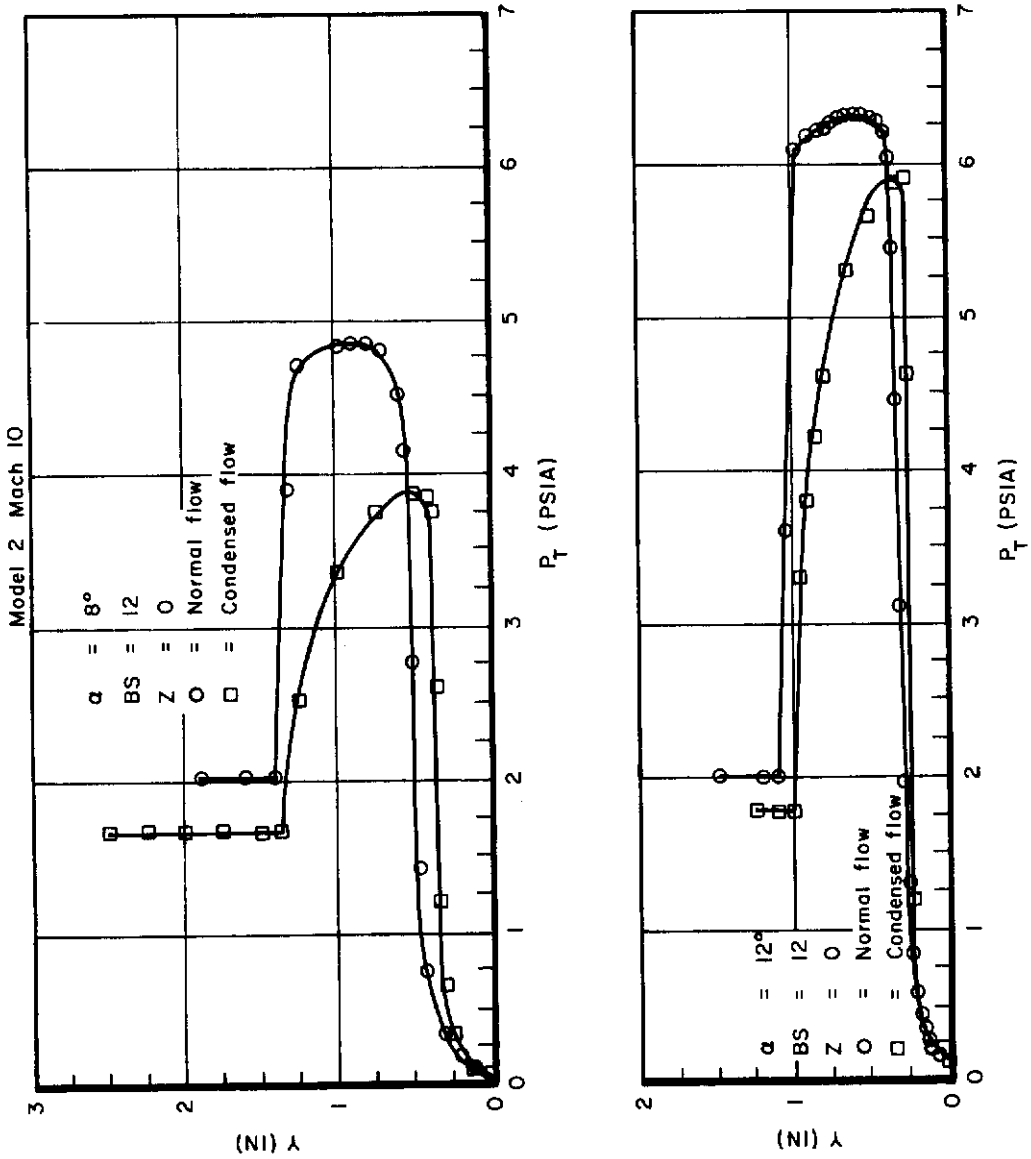

Figure 5. Effects of Condensed Flow on Pitot Pressure Profiles

After it had been determined that condensation does affect both the inviscid and viscous flow, the vapor screens were further examined with the realization that direct comparisons between the standard and condensed flows could not be made.

The vapor screens on the 18-inch, blunt 70° model, which have been sketched in Figure 6, show the location of the aft shock region as a lighter area which is a result of increased density behind the shock. They also show a dark, almost black, region near the model surface. The most interesting feature of the vapor screens is the shape of the dark region, particularly the hump seen on the center line at the near portion of the model. The hump along the center line (Figure 6) was thought to be a blunt nose induced phenomenon so a series of vapor screen runs were made on the sharp nose, sharp leading edge Model 3. In these photographs (Figure 7) the camera-model orientation did not allow good definition except at the 24- and 30-inch body station. Here, the center line hump is still evident at angles of attack of 0, 4 and 8 degrees, though only a slight trace shows at $\alpha = 8°$.

Vapor screens were also made with the blunt 80°delta Model 5 but due to the relatively narrow span and dim light conditions, quantitative measurements were not possible. However, the center line hump was again evident in the dark region.

Therefore, it appears from the data and analysis of this study that flow phenomena during condensed free stream conditions are different than those during standard operating conditions and that direct comparisons between the two cannot be made. Even comparisons between vapor screen photographs and pitot pressure surveys during condensed flow did not correlate. This may be due in part to errors introduced while measuring distance in the vapor screens with their dim lighting conditions and various model-camera orientations. There is also a question of interpretation of vapor screens; the only identifiable item in the vapor screens taken during this study is the shock wave, though some investigators have been able to identify vortices in vapor screens of lee-side flow fields.

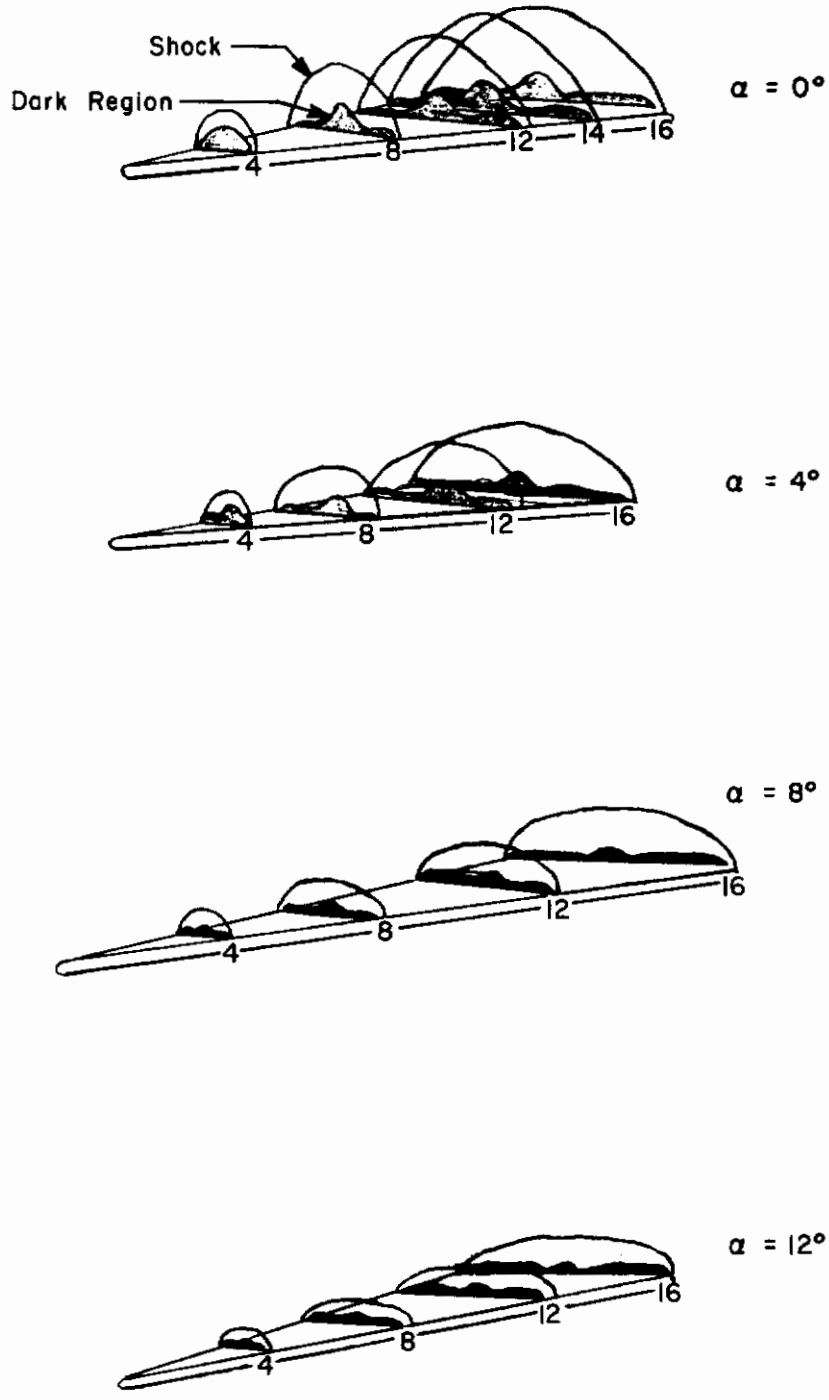

Figure 6. Sketches Of Vapor Screens Of Model 2 at Mach 10

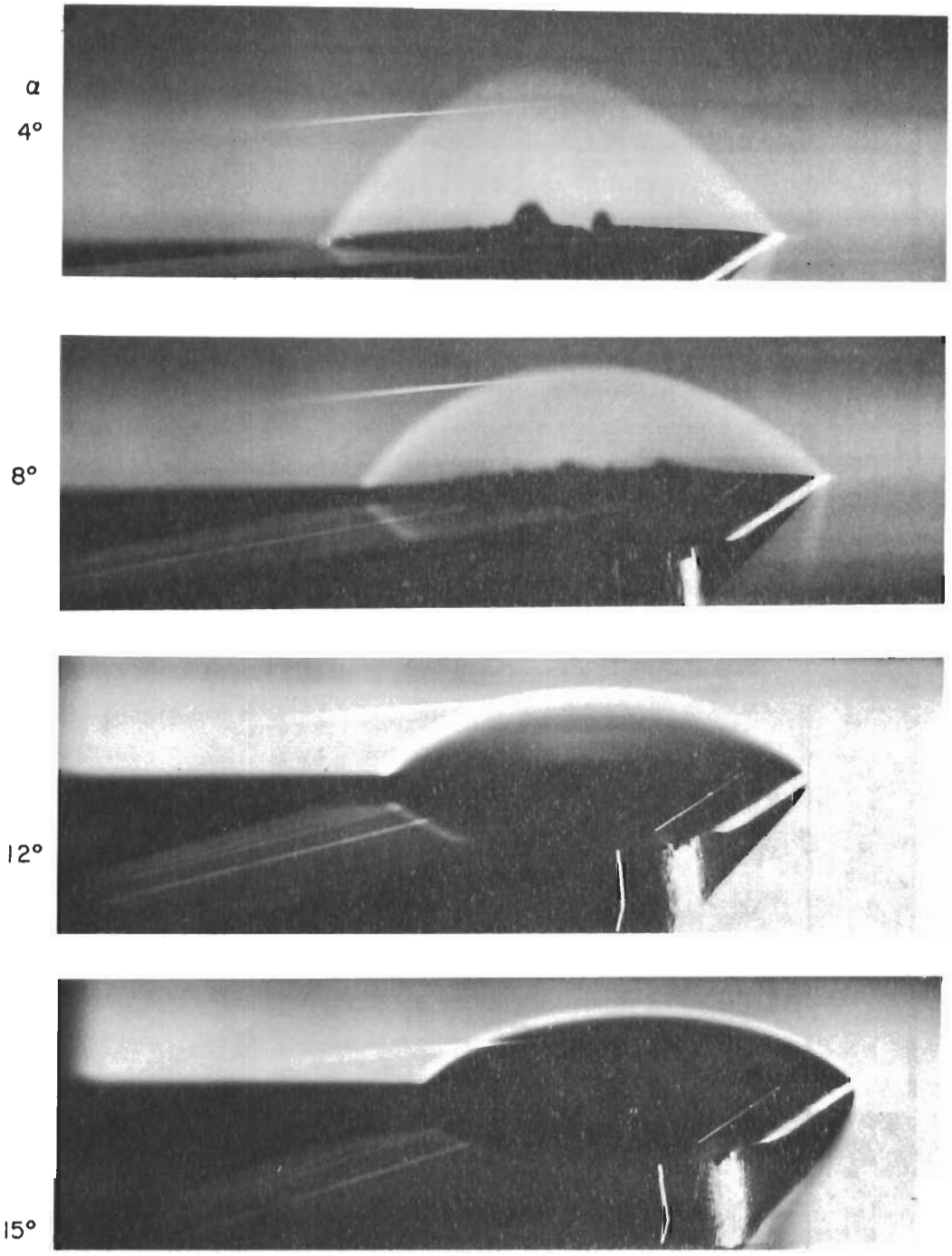

X = 24 inches

Figure 7a. Vapor Screens of Model 3

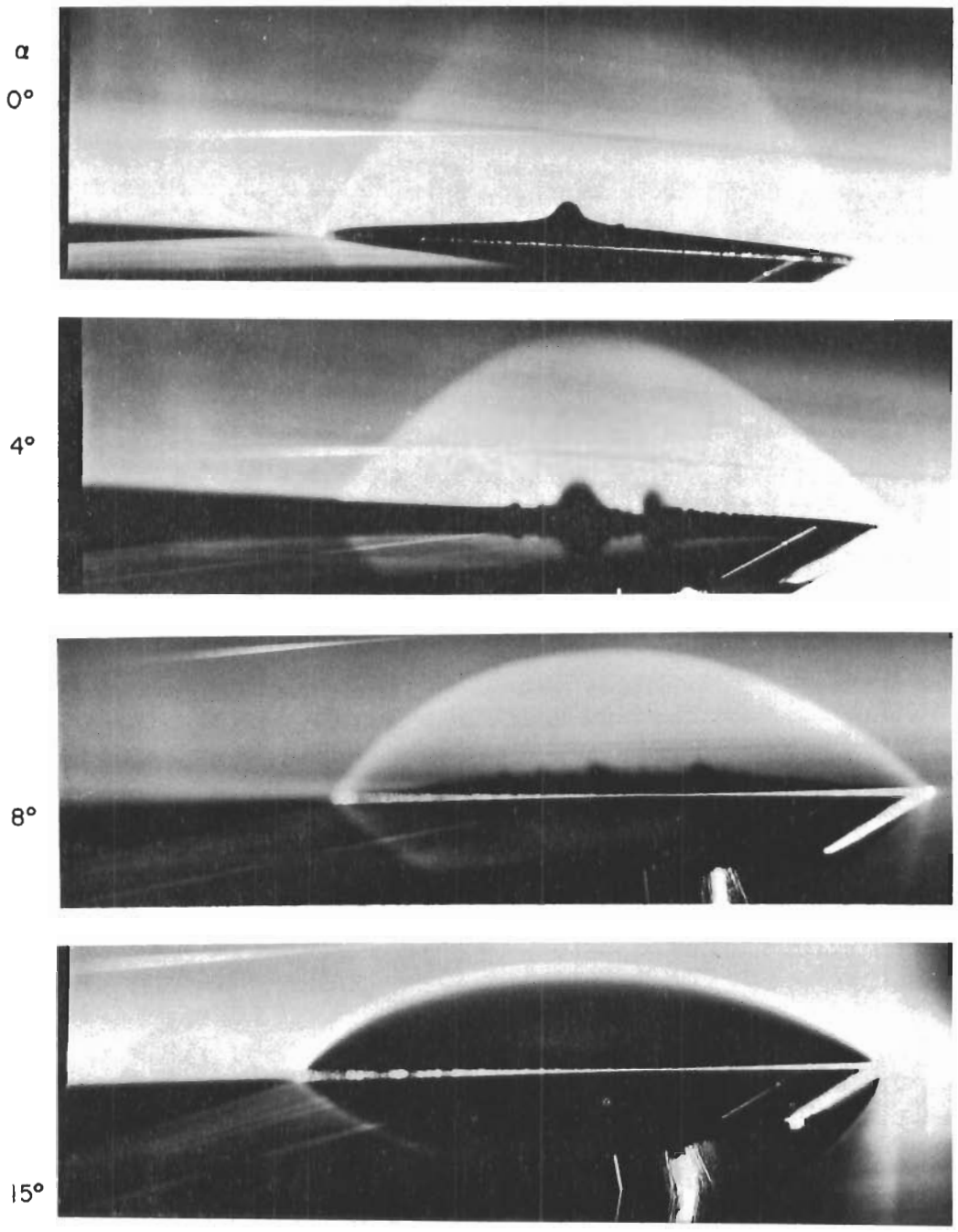

X = 30 inches

Figure 7b. Vapor Screens of Model 3

One further comment about vapor screens; better model definition was obtained when both the camera and light source were on the same side of the model surface of interest and also on the same side of the wind tunnel. When both are on the same side of the model, the camera views the strip of light as it crosses the model defining the model extremities. When both were on the same side of the wind tunnel, there seemed to be less glare in the photographs, again allowing better definition of the model and flow details.

2. PITOT PRESSURE SURVEYS

a. On Center Line

Center line pitot pressure profiles on the 80° Model 5 are shown in Figures 8 to 10. From these profiles, it can be seen that three distinct regions can be described and, depending on the particular angle of attack and distance from the blunt nose, each profile can demonstrate from one to all three of these regions.

The first (inner) region is one of constant pitot pressure adjacent to the model surface and consists of the flow which passed through the normal part of the bow shock wave with subsonic flow behind it and has experienced the greatest entropy loss. The second (middle) region is characterized by a large pitot pressure gradient which corresponds to the flow which passed through a curved, low-angle shock wave with supersonic flow behind it. The entropy loss of this flow varies with the distance from the model. The third (outer) region is also characterized by a constant pitot pressure and consists of flow which passed through the zero strength Mach line.

Calculations and measurements of shadowgraphs and schlierens were made to help describe and delineate the various regions of the flow. Measurements were made of the boundary, entropy, and shock layer thicknesses and the apparent heights have been labeled on the figures. The equations of Reference 28 were used to calculate a pitot pressure distribution as a function of shock wave angle. This was accomplished by processing the flow through the shock, isentropically expanding it from the aft-shock conditions to a downstream static pressure (assumed constant normal to the surface) and then calculating normal shock pitot conditions at the local Mach number as would be measured by a pitot tube at that location in the flow. The major points which are indicated on

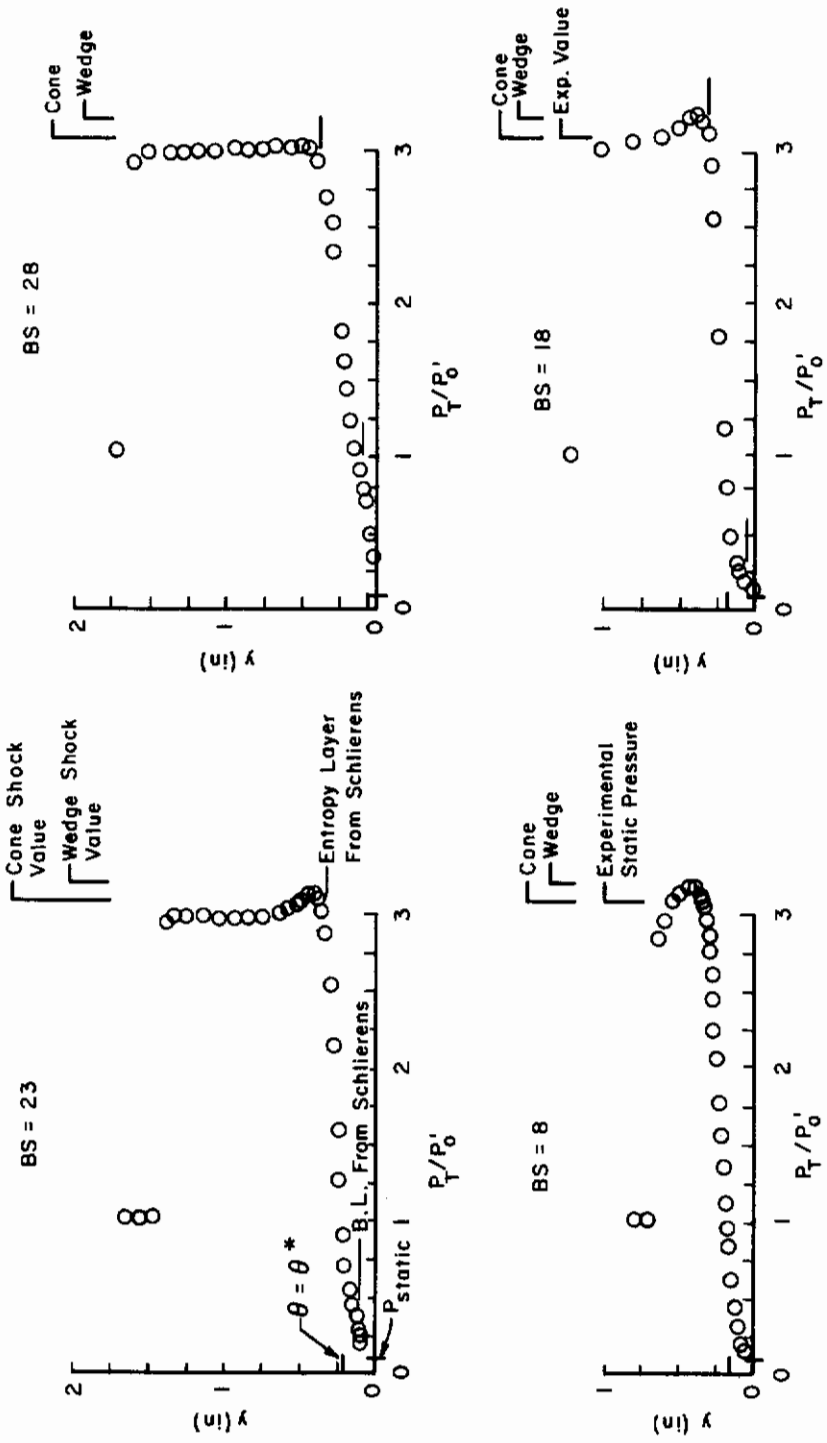

Figure 8. Mach 8 Pitot Profiles on Model 5 at $\alpha = 14°$

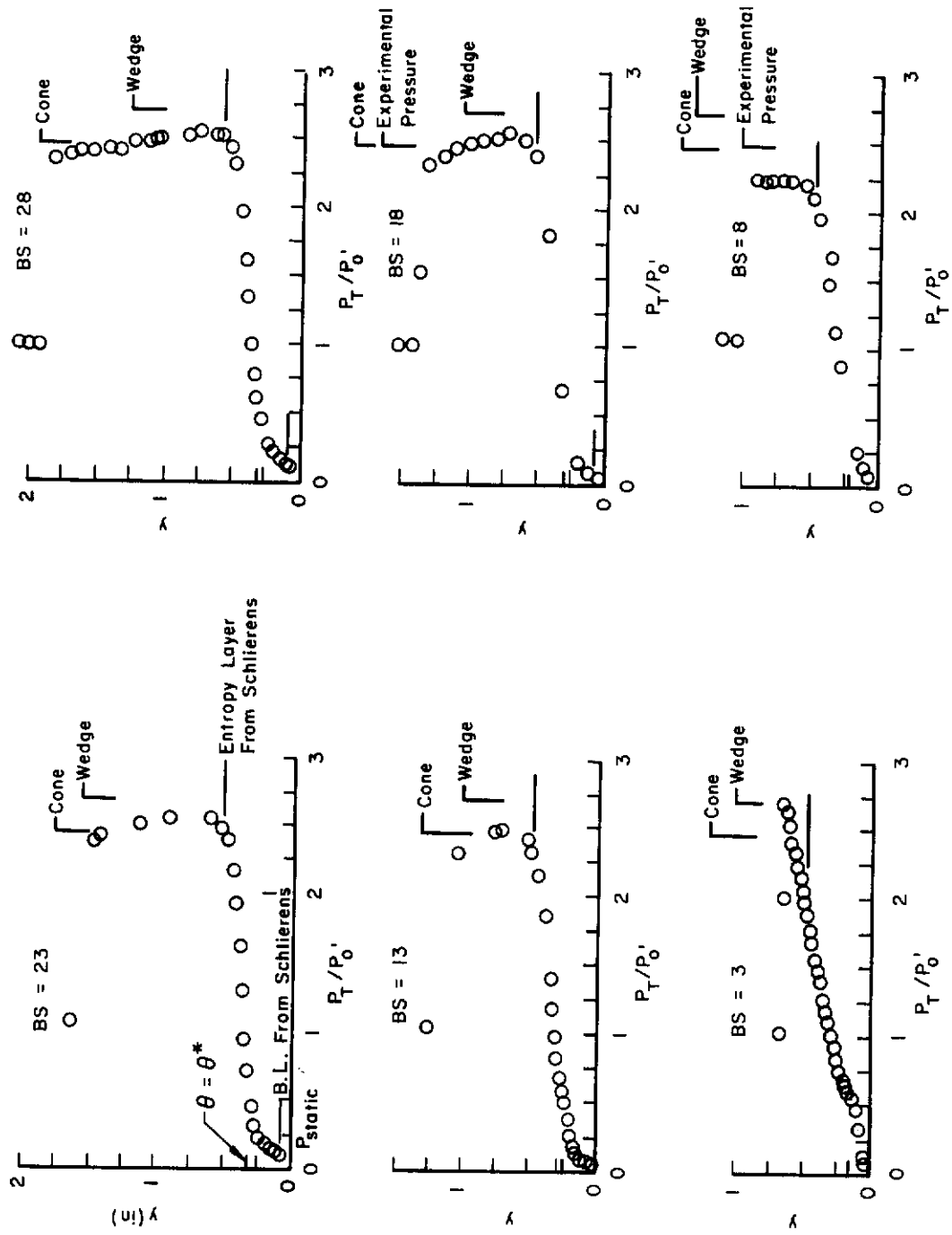

Figure 9. Mach 8 Pitot Profiles on Model 5 at $\alpha = 10°$

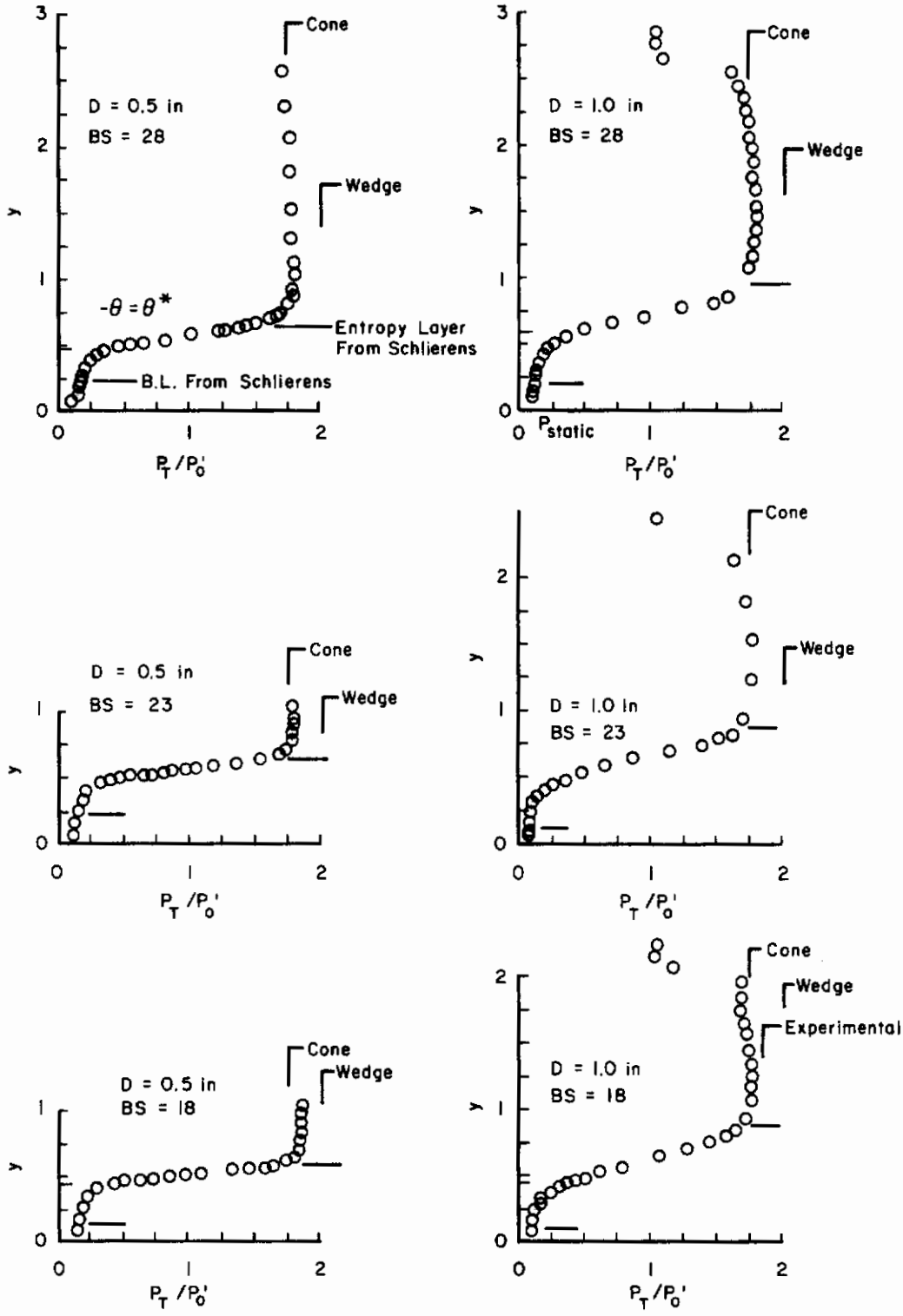

Figure 10. Mach 8 Pitot Profiles on Model 5 at $\alpha = 6°$

the figures are the pitot pressure ratios corresponding to wedge and cone shocks and the value corresponding to the shock angle with sonic flow behind sonic flow behind the shock. It has arbitrarily been decided herein that this point and its expanded stream line down stream separates the normal shock entropy flow from the oblique shock entropy flow.

The figures show two horizontal lines which seem to separate the three regions. The "θ^* line", which corresponds to the predicted θ^* pitot pressure, is located near the lower knee of the curve and bounds the inner region. Within the region, the analytical method predicts a nearly constant pitot pressure as seen in the figures, but the predicted value is near the θ^* value which is higher than the measured value. It could be possible that the boundary layer is affecting the pitot distribution, but measured boundary layer thicknesses taken from schlierens (Figures 11 to 14) and shadowgraphs are seen to be half (or less) the distance to the θ^* line. The measured pitot pressure between the boundary layer and the θ^* line is less than predicted. Even for $\alpha = 6°$, with the thickest constant entropy layer, there is no measured effect of the boundary layer on the pitot pressure.

The lower bound of the outer region is marked by a line which represents the edge of the variable entropy layer. This line can be seen in schlierens (Figures 11 to 14) as the junction of light and dark areas indicating a density gradient which would be calculated using the measured pitot profiles. There is some question that the maximum density gradient as indicated in the schlierens is actually inside the outer edge of the variable entropy layer but the figures show the "measured" height is inside if not on the upper knee of the curve. The magnitude of the pitot pressure in the outer region agrees very well with the conical prediction method. At Body Stations 8 and 18, where surface pressures taps were located, predictions have been made based on measured static pressures. These predictions are in good agreement with both the measured and conical pitot pressures.

b. Off Center Line

The off center line pitot surveys demonstrated some unexpected distributions. Mach 8 plots are shown in Figures 15 to 20. The distributions

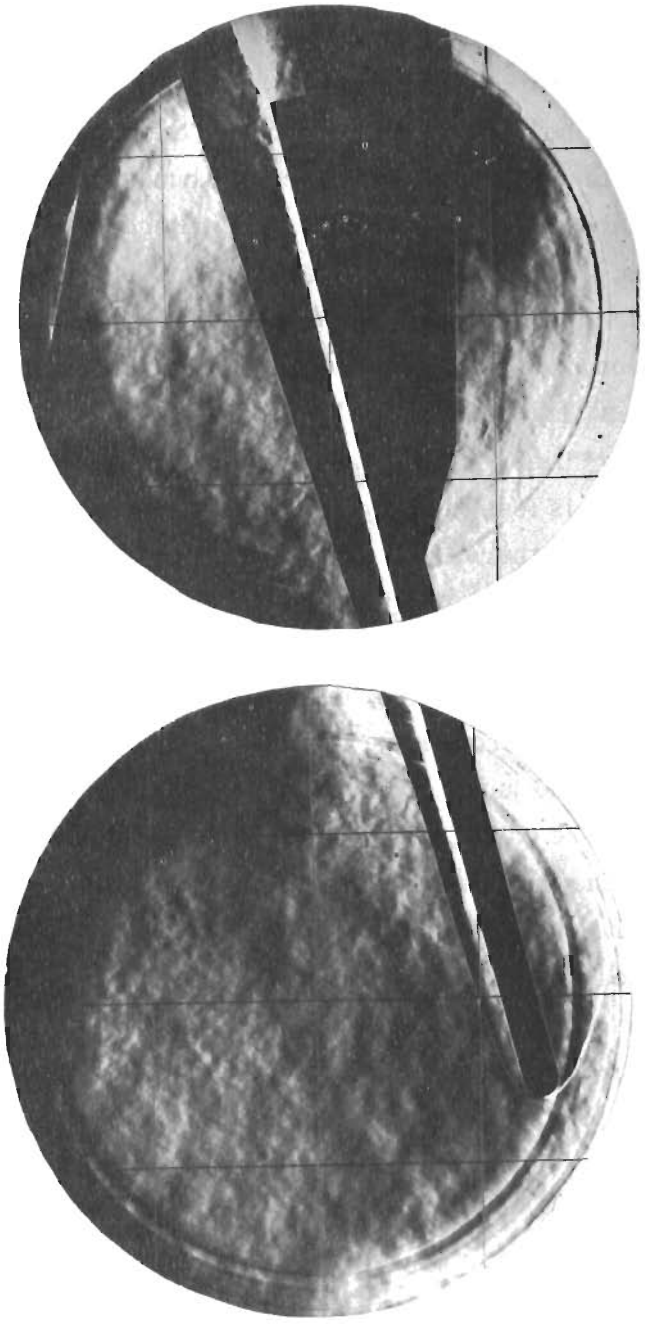

Figure 11. Schlieren Photograph of Model 5, α = 14° at Mach 8

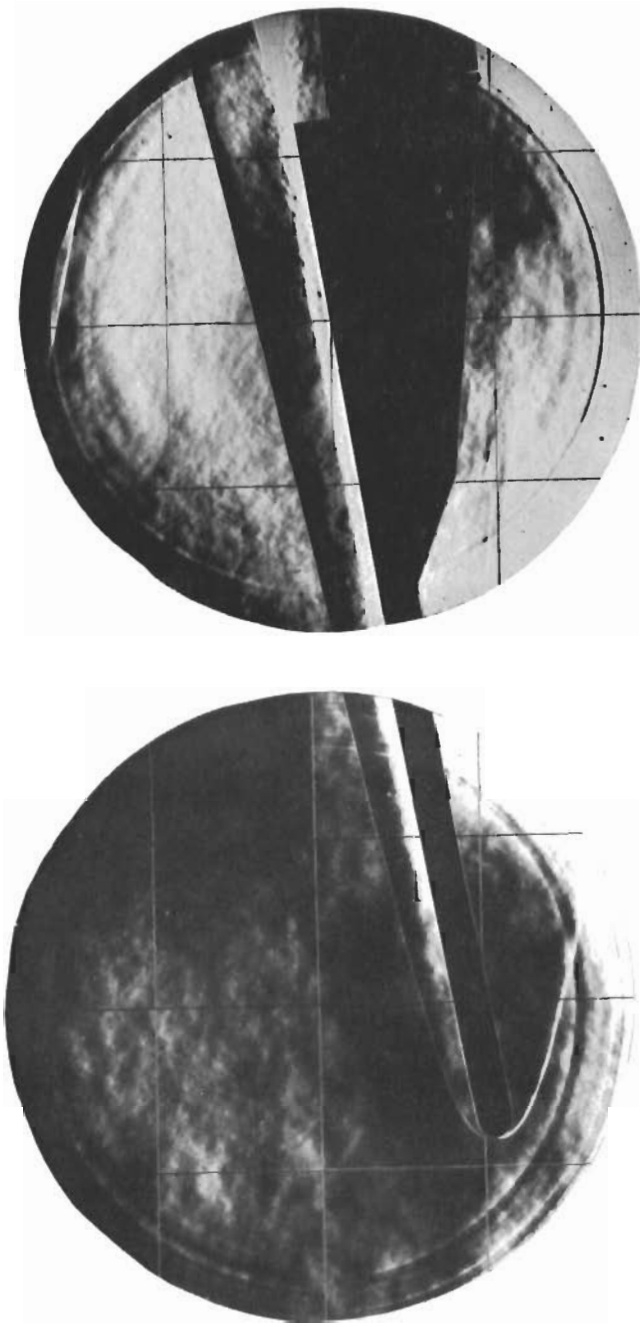

Figure 12. Schlieren Photograph of Model 5, α = 10°at Mach 8

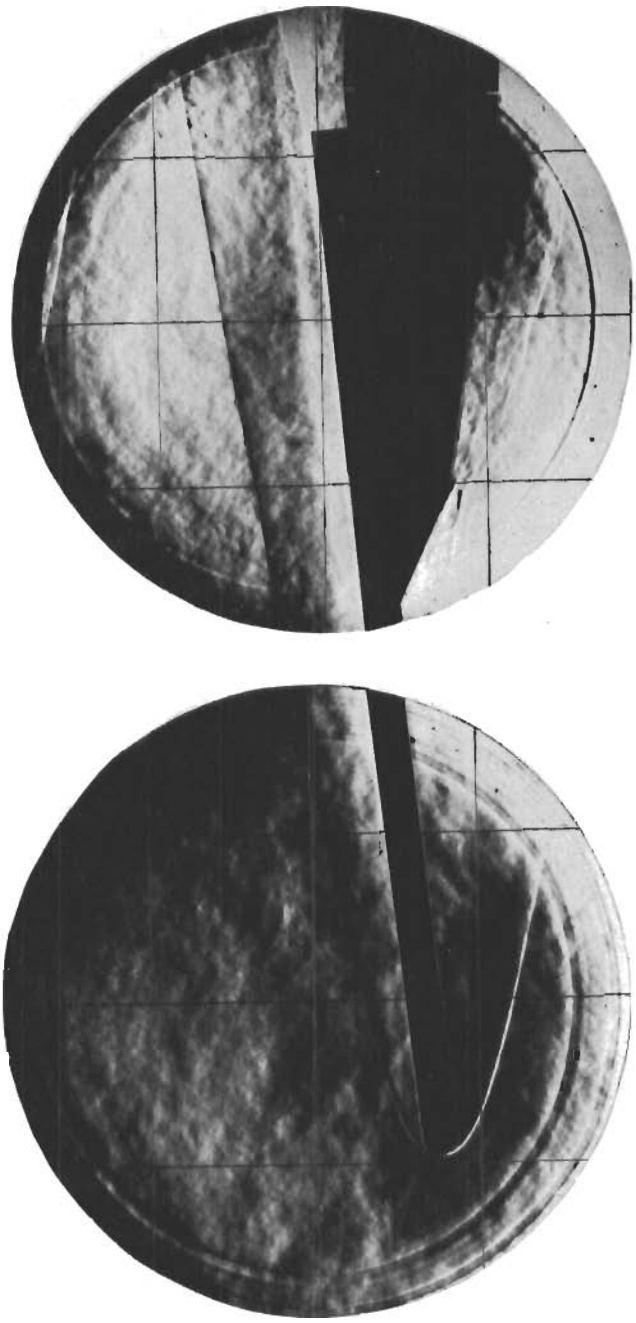

Figure 13. Schlieren Photograph of Model 5, $\alpha = 6^{\circ}$ at Mach 8

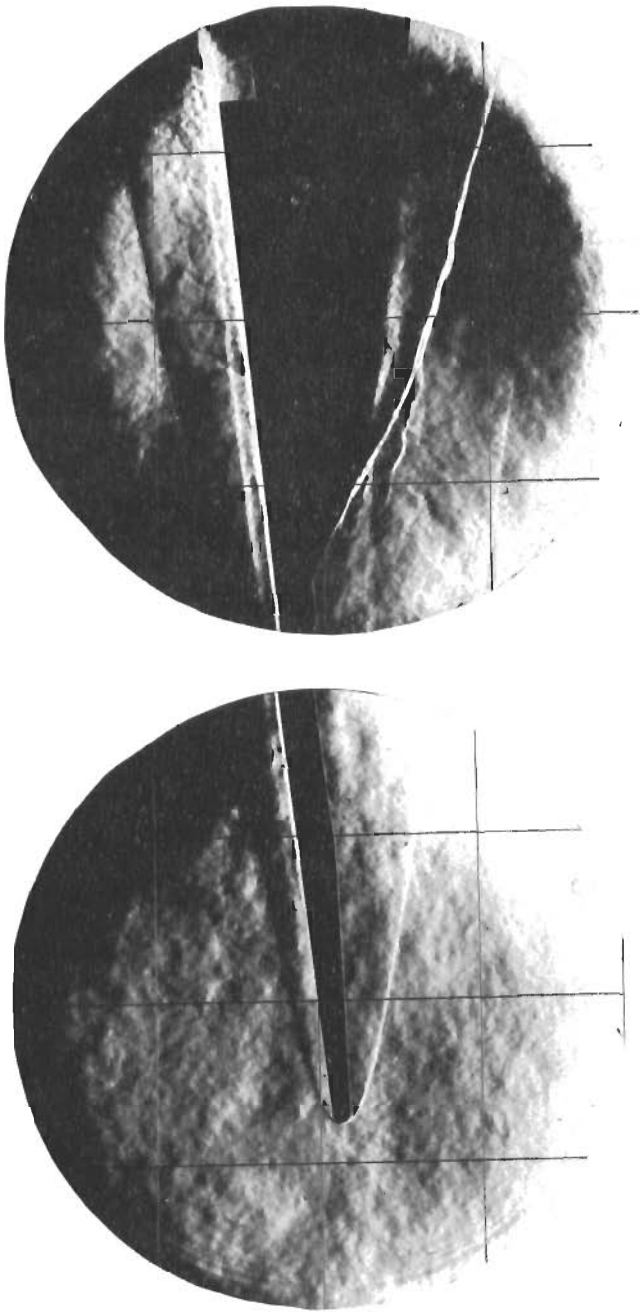

Figure 14. Schlieren Photograph of Model 5, α = 6° at Mach 8, .25 Inch Radius

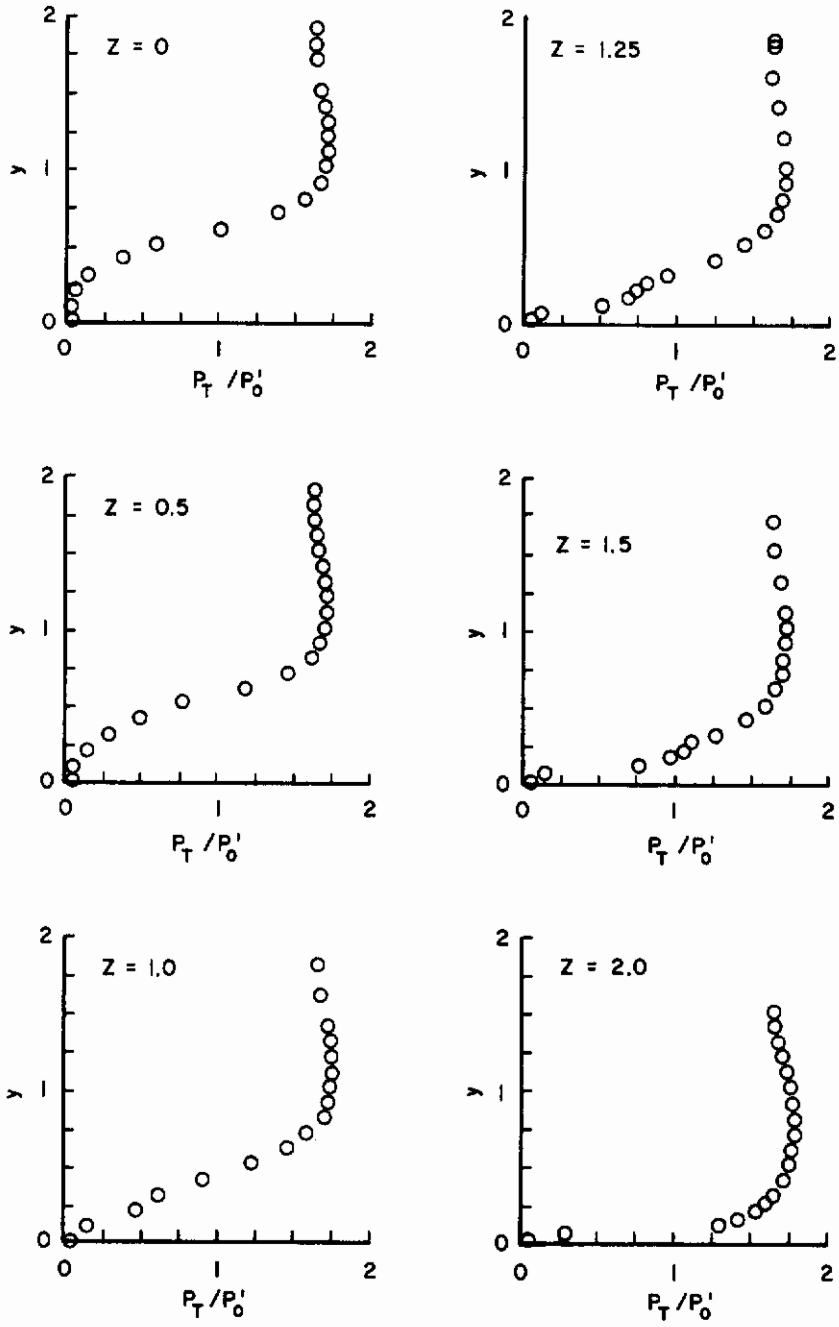

Figure 15. Off Center Line Pitot Profiles on Model 5, Mach 8, α = 6°, BS = 18

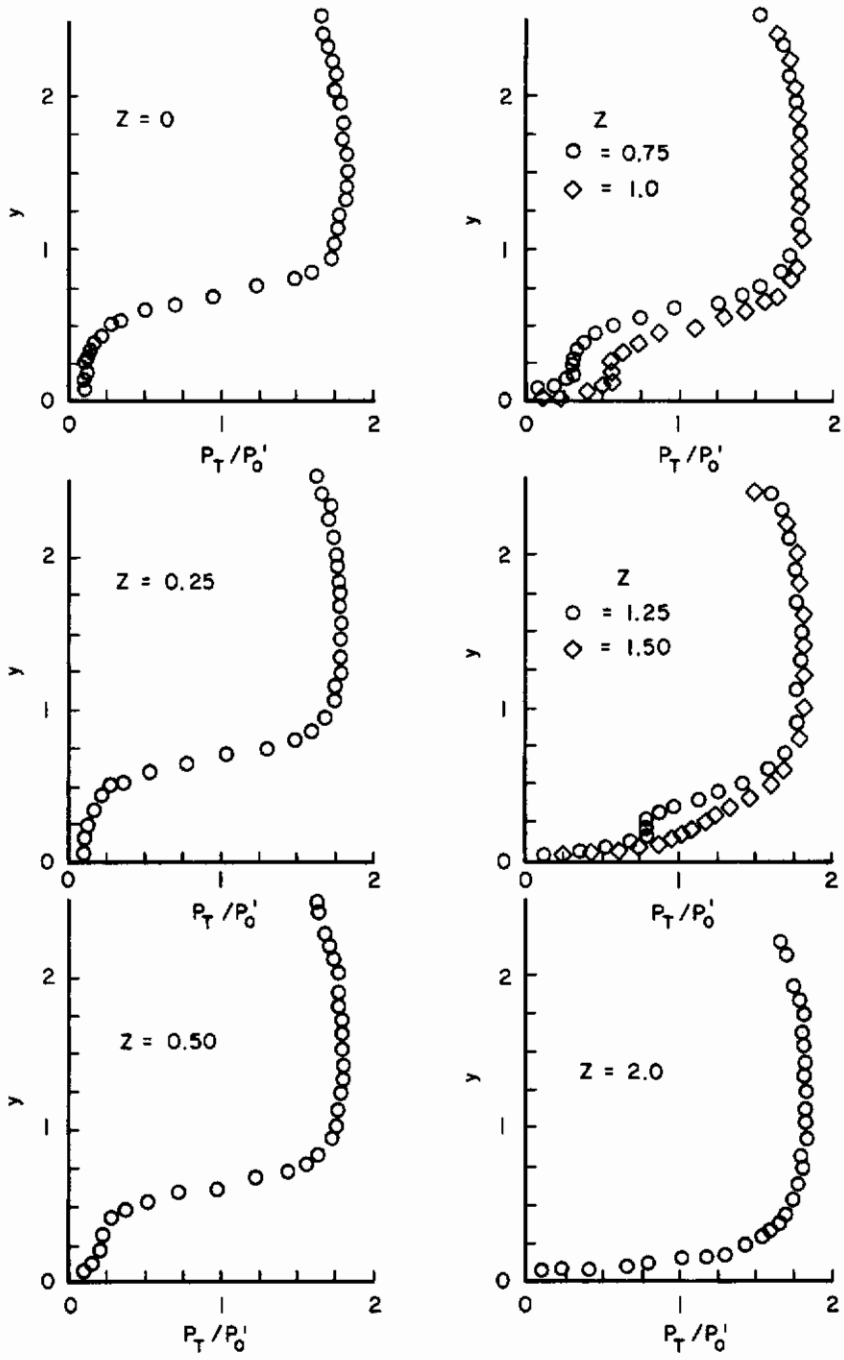

Figure 16. Off Center Line Pitot Pressure Profiles on Model 5, Mach 8, α = 6°, BS = 28

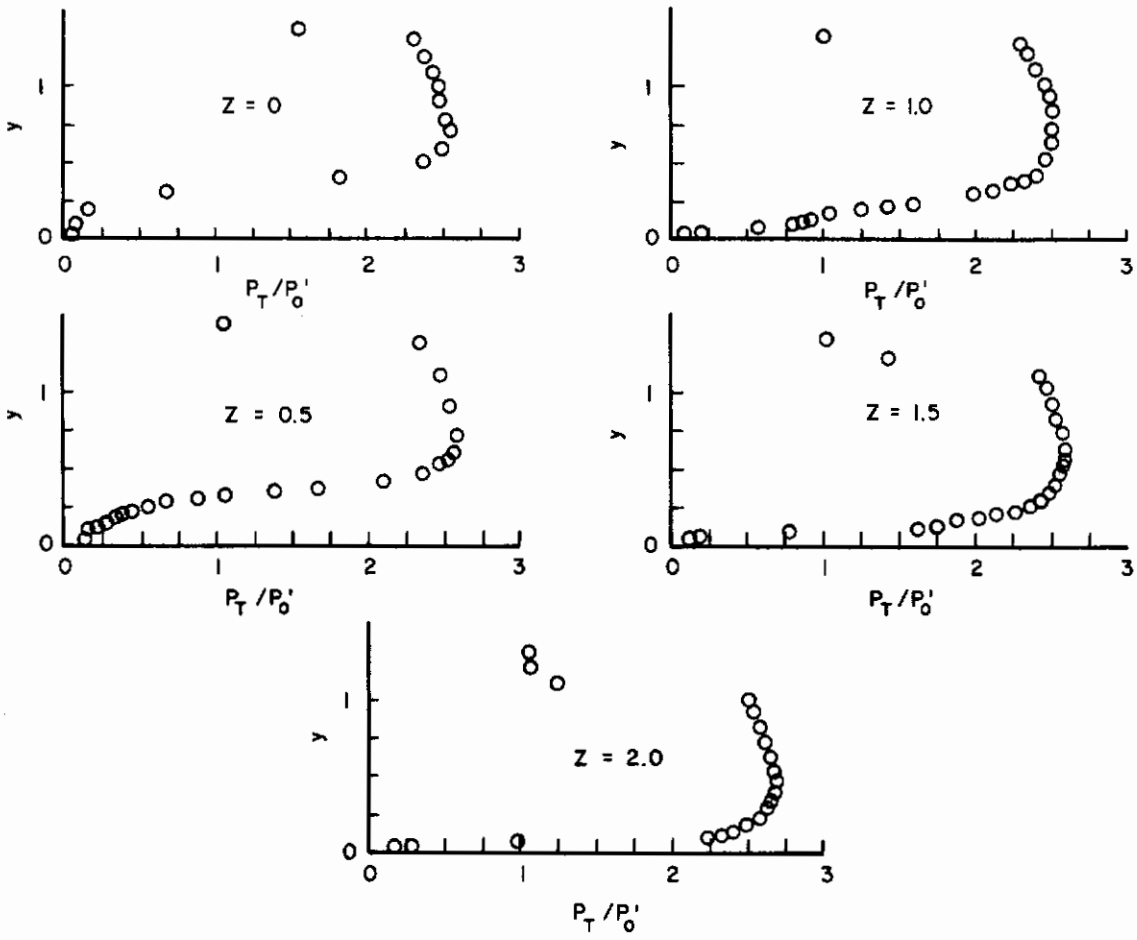

Figure 17. Off Center Line Pitot Pressure Profiles on Model 5, Mach 8, α = 10°, BS = 18

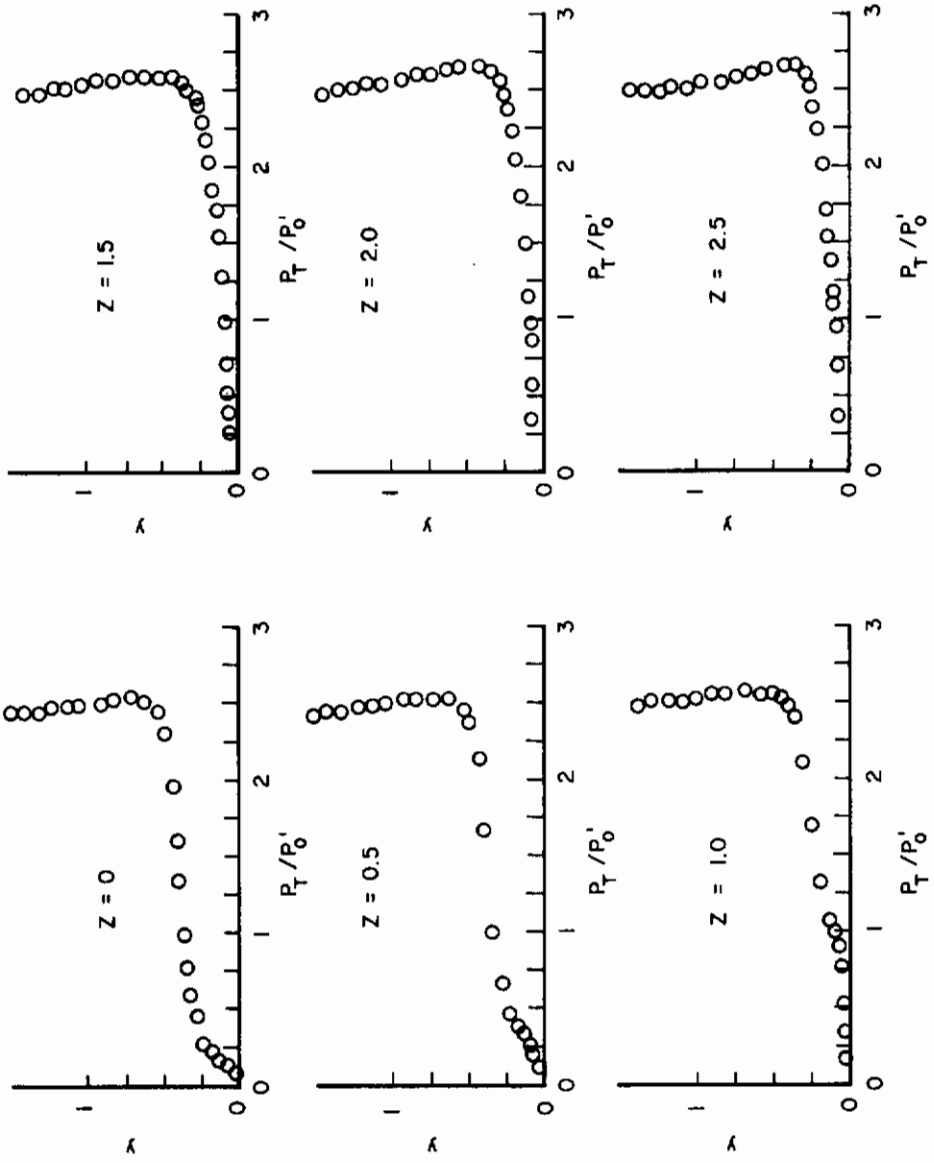

Figure 18. Off Center Line Pitot Pressure Profiles on Model 5, Mach 8, α = 10°, BS = 28

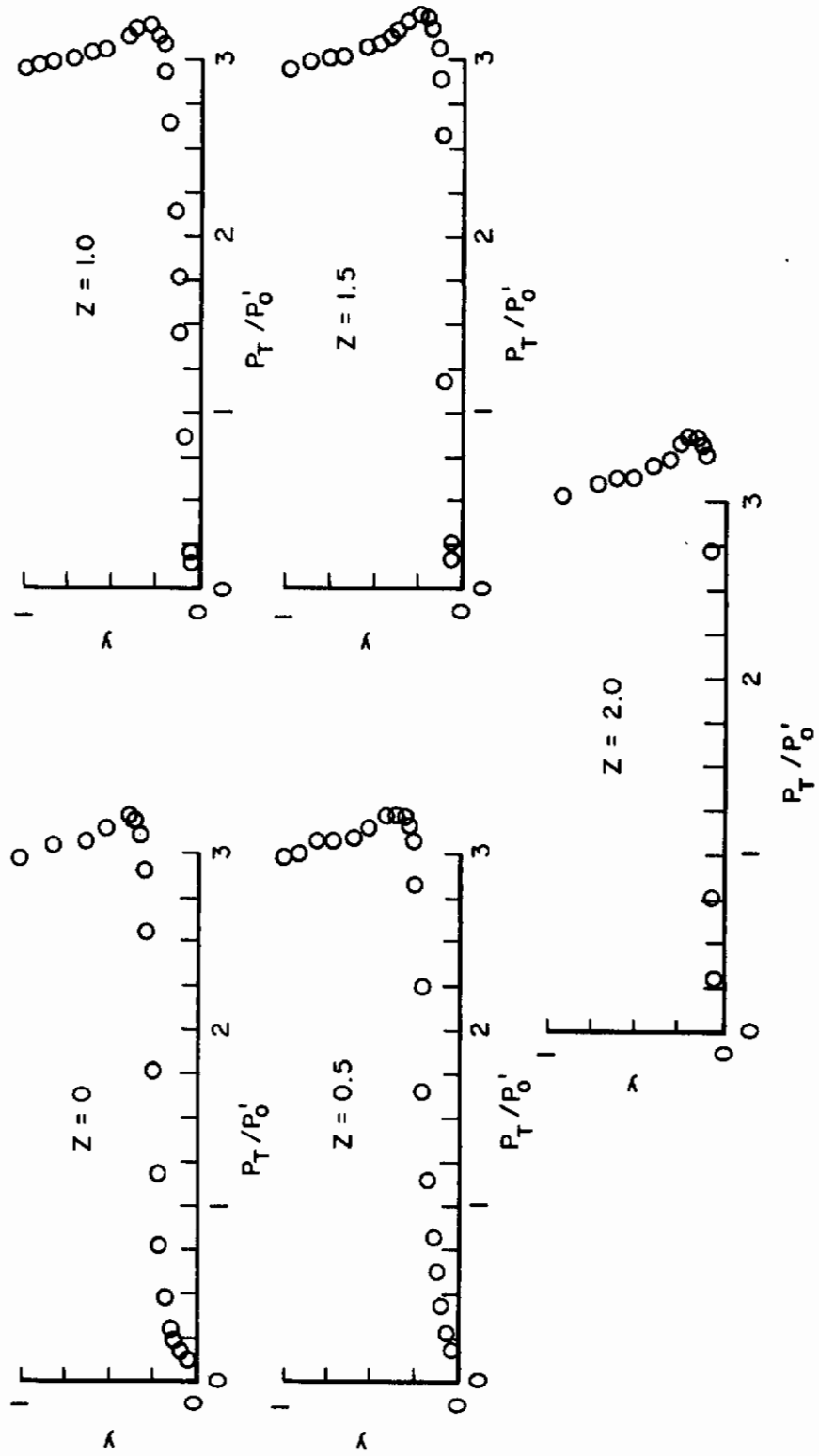

Figure 19. Off Center Line Pitot Pressure Profiles on Model 5, Mach 8, α = 14°, BS = 18

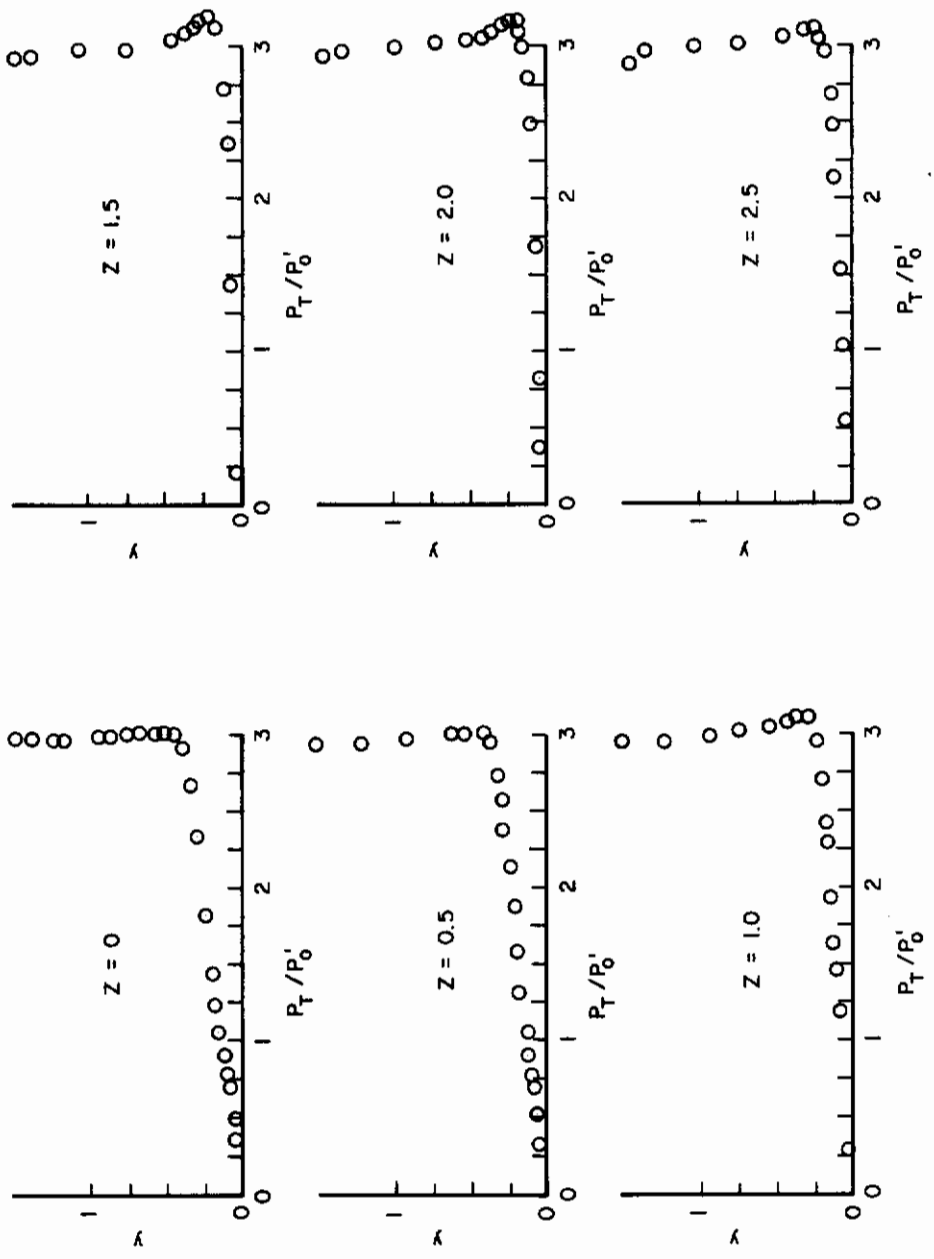

Figure 20. Off Center Line Pitot Pressure Profiles on Model 5, Mach 8, α = 14°, BS = 28

for $\alpha = 6$ at BS 18 in Figure 15 show that near the center line the pitot profiles are similar to those on the center line. The distributions farthest from the center line are more similar to a sharp flat plate profile without the normal shock entropy adjacent to the surface. The unexpected distributions are seen for $\alpha = 6$, BS 28 in Figure 16. The profiles nearest and farthest from the center line are the same as those at BS 18. However, at midspan distances from .5 to 1.25 inches, there appears to be a combining of the two distributions with the swept leading edge oblique shock entropy flow next to the model surface and the normal shock entropy flow above it. This merging of the two flow fields can also be seen in the oil flow photograph (Figures 21 to 23). At $\alpha = 6°$, (Figure 21) and BS 28, the flow on the center line is strip wise while inflow is seen off the center line and a merging region is evident. A line describing the merging region can be extended upstream. (Such a line has been indicated by the white dots in the figure.) The indicated line is not straight as might be expected but this could be a result of oil dots which are not uniform in size and depth and affected differently by the local shear of the flow field. The merging of the two flow fields at BS 18 as seen in the pitot profiles (Figure 15) is not as obvious as at BS 28, but there is a slight inflection between Z = 1.0 and 1.5 which is probable evidence of it. Inflections can also be seen in the remainder of the profiles (Figure 17 to 20) except BS 18 at $\alpha = 14°$ (Figure 17) where the pitot gradient is very large near the surface and the inflection is not evident.

The oil flow photograph for $\alpha = 10°$ (Figure 22) shows a slight indication of the merging flow fields but none is discernible at $\alpha = 14°$ (Figure 23). In fact, at $\alpha = 14°$ and particularly at rear of the model, there appears to be flow across the model center line. It can be observed in all three oil flow pictures that the inflow is most obvious on the forward part of the model but the pitot profiles best demonstrate the merging flow fields at BS 28 where the oil flows are less discrenible. Another noteworthy comment about the oil flows, and this again could be a result of nonuniform oil drop sizes, is that there is greater shear (longer oil streaks) on the outboard part of the model than on the center line. The pitot profiles also show a greater shear (pitot gradient) off the center line.

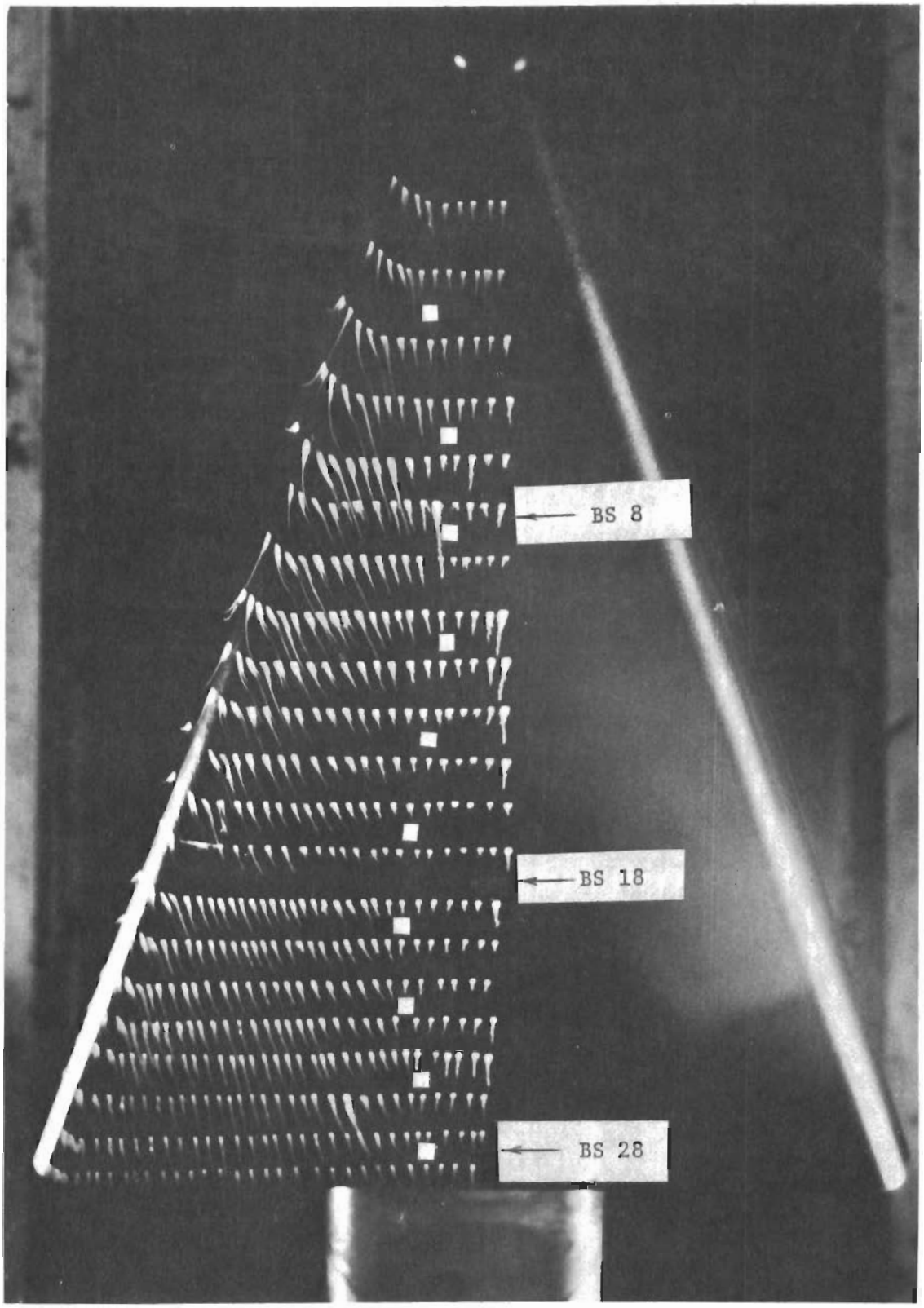

Figure 21. Oil Flow Photograph of Model 5 at Mach 8, α = 6°, $R_{e\infty}$ /ft = 2 x 10^6

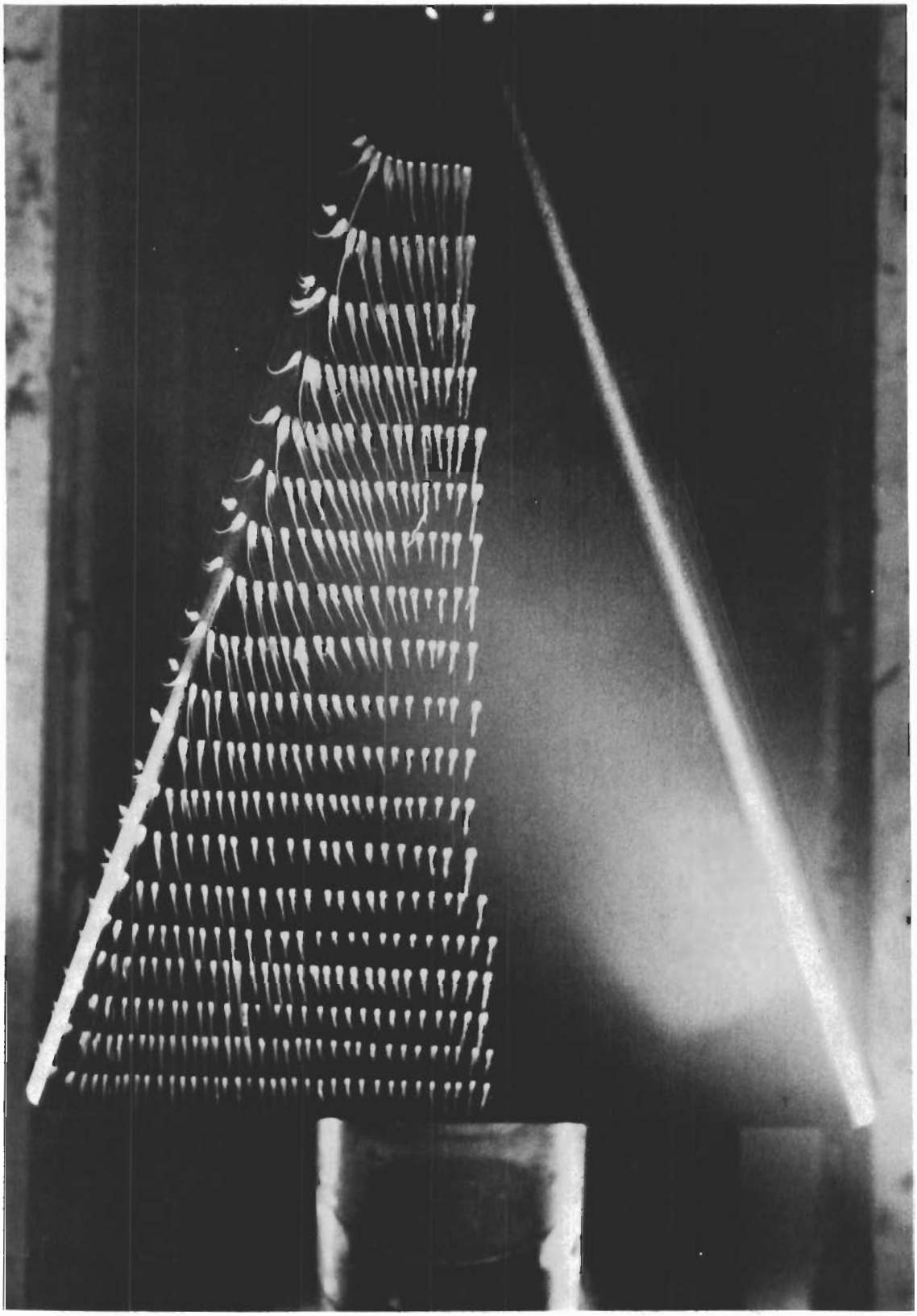

Figure 22. Oil Flow Photograph of Model 5 at Mach 8, α = 10°, $R_{e\infty}$ /ft = 2 x 10^6

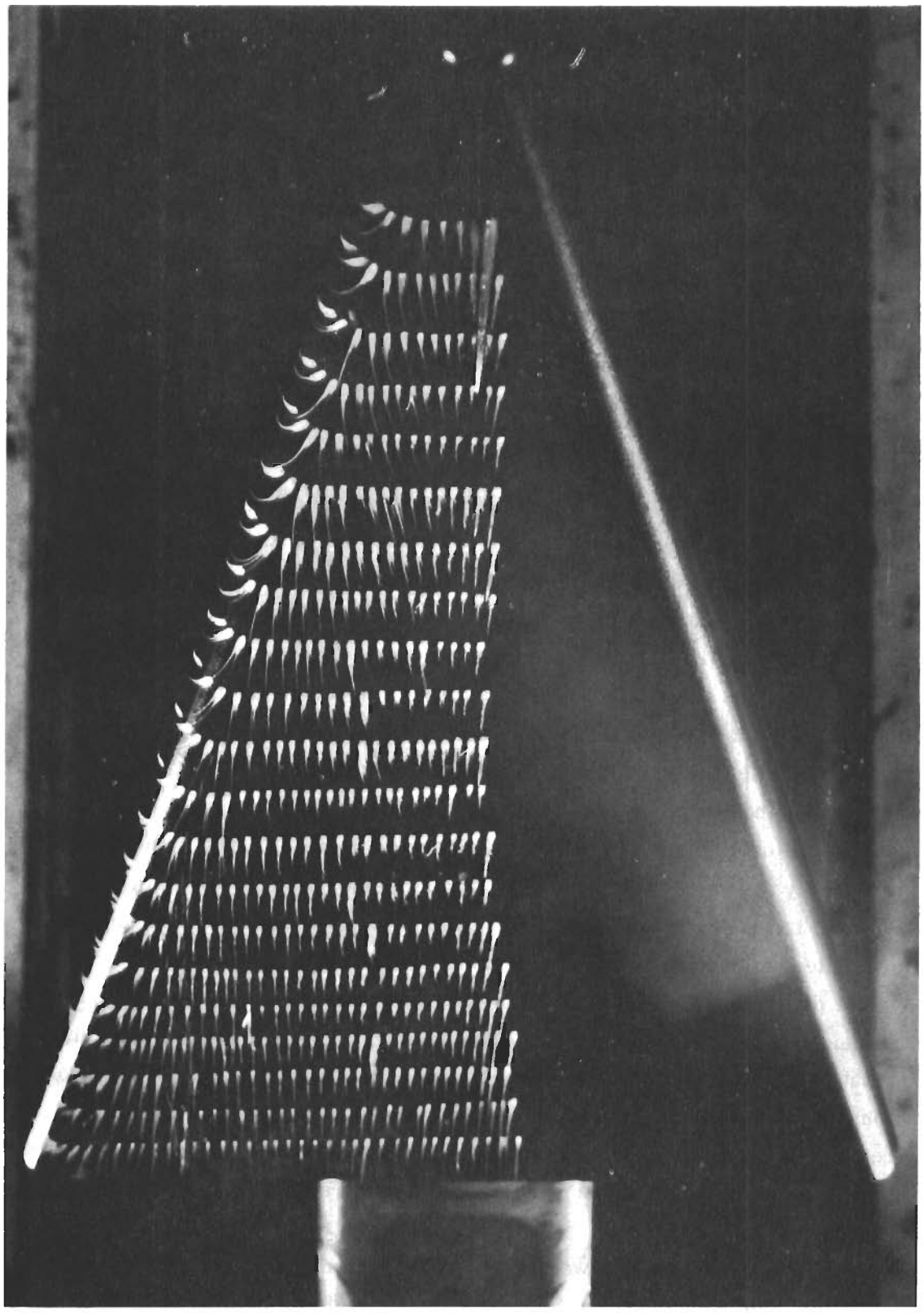

Figure 23. Oil Flow Photograph of Model 5 at Mach 8, α = 14°, $R_{e\infty}$/ft = 2 x 10^6

3. HEAT TRANSFER DISTRIBUTION

Referring to the oil flow pictures in Figures 21 to 23, it can be seen that flow is expanding over the leading edge onto the lower surface at $\alpha = 6°$. At the rear corner of the model at $\alpha = 10°$, the flow is beginning to turn outward over the leading edge while inflow exists on the forward part. The same thing is happening at $\alpha = 14°$, only a greater portion of the lower surface is affected by outflow. This would lead one to believe that the leading edge stagnation line leaves the leading edge and becomes a "divergence" stream line on the lower surface with inflow toward the center line on one side and outflow toward the leading edge on the other. The movement of such a line would determine the existence of inflow and outflow on a slab delta wing lower surface.

If the stagnation line does leave the leading edge and extend across the lower surface, the heat transfer distribution along the leading edge-lower surface tangency line should show a local maximum where it is crossed. A distribution has been plotted in Figure 24 for Mach 8 and it can be seen that a maximum does exist and that its location moves forward with increasing angle of attack as does the "divergence streamline" of the oil flows. The location of the local peak is given as a function of angle of attack in Figure 25 for a range of Mach and Reynolds number. It can be seen that, except for a possible Mach number dependency at α less than eight degrees, there is apparently no dependence on either Mach number of Reynolds number. The Mach number dependency at low angle of attack is not a certainty because the peak becomes very flat in this range and is difficult to locate. Attempts were made to correlate the location of the peak tangency line heating with the oil flow pictures, but the determination of the locus of the divergence streamline, the location of the tangency line, and their intersection, is subject to a great deal of interpretation. The locations measured in the oil were greater than those taken from the heating data (Figure 25). There could be combining effects of pressure and velocity gradients to cause the heat transfer to peak at a point other than one would imagine from stream line directions.

Since no pressure data were taken along the tangency line of this model, the data of References 29 and 30 were examined (data obtained under private communication with authors) to determine whether there is a similar effect on

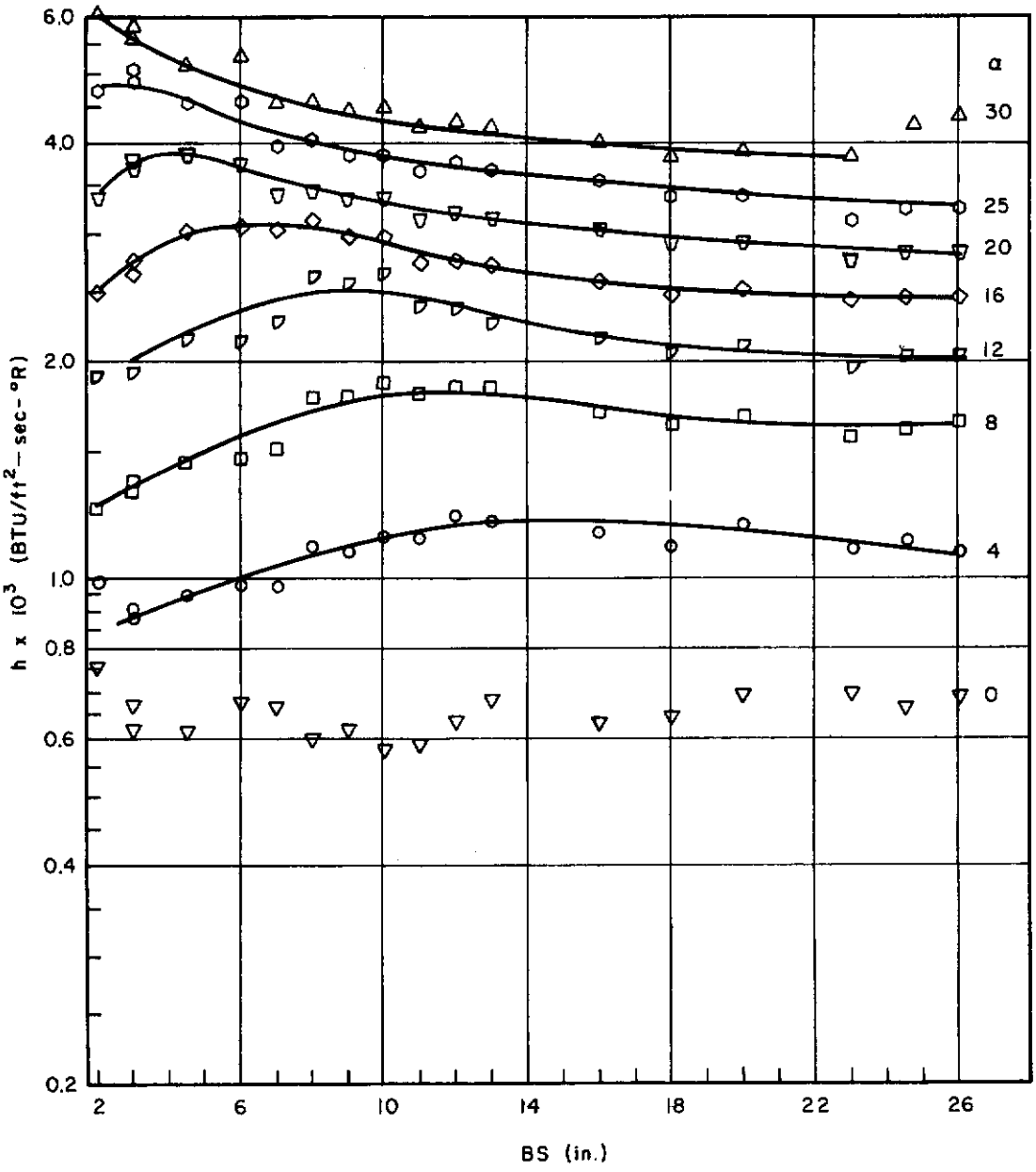

Figure 24. Leading Edge - Lower Surface Tangency Line Heating on Model 4, Mach 8, Re_∞ /ft = 2 x 10^6

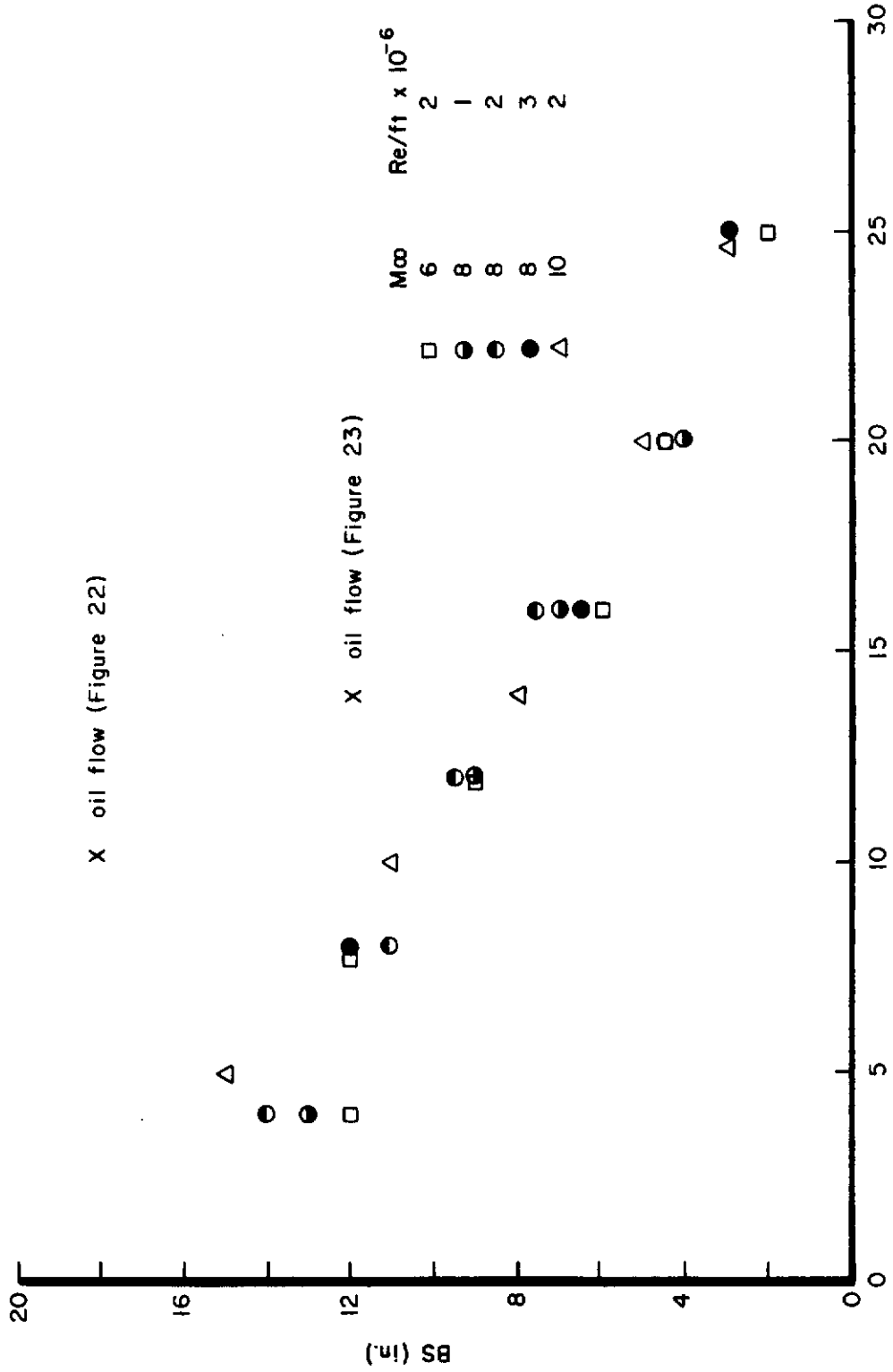

Figure 25. Location of Local Peak Tangency Line Heating on Model 4

the pressure distribution. These data proved to be extra valuable in that both sharp and blunt nosed models were tested and the effect of nose shape could be studied.

Heat transfer and pressure data on the blunt nose model of Reference 29 are shown in Figures 26 and 27. Local peaks in the heat transfer data are seen, but their movement forward with angle of attack is not smooth. Some of the forward thermocouples seemed to be reading erratic data and there was not a sufficient number of remaining thermocouples to obtain a good distribution. The blunt nose pressure data (Figure 27) do not show a similar maximum or a movement with angle of attack. In fact, for the angle of attack range (10 to 25°) in which the heat transfer reaches a peak within the instrumented limits of the model, the pressure distribution is generally flat. For the sharp nose model (Figures 28 and 29), there is an increase in the tangency line heating, but the increase is very slight and its location does not change as the angle of attack is increased. Therefore this peak cannot be related to that seen on the blunt nose model. Pressure data on the sharp nose model is the same as on the blunt model.

The sharp and blunt heat transfer data from Reference 30 (Figure 30) show more clearly the different effects of nose shape on the tangency line heating distribution. The sharp nose data are generally flat but the blunt data show a definite peak which moves forward with angle of attack.

The continuation of this divergence streamline onto the lower surface can be seen in the spanwise heat transfer distributions in Figure 31 for Model 4 at Mach 8 and Re/ft = 2×10^6. The heating parameter plotted is a ratio of experimental to theoretical heat transfer coefficients where the theoretical heating is based on the reference temperature method with sharp wedge pressure and an effective reference length measured chordwise from the leading edge. This parameter was used mainly to collapse the length dependence of the data and to nondimensionalize them, not as a correlation parameter.

In the angle of attack range from 6 to 16°, it can be seen that there is a local peak in the off-center line heating at body station 18 and a hint of an

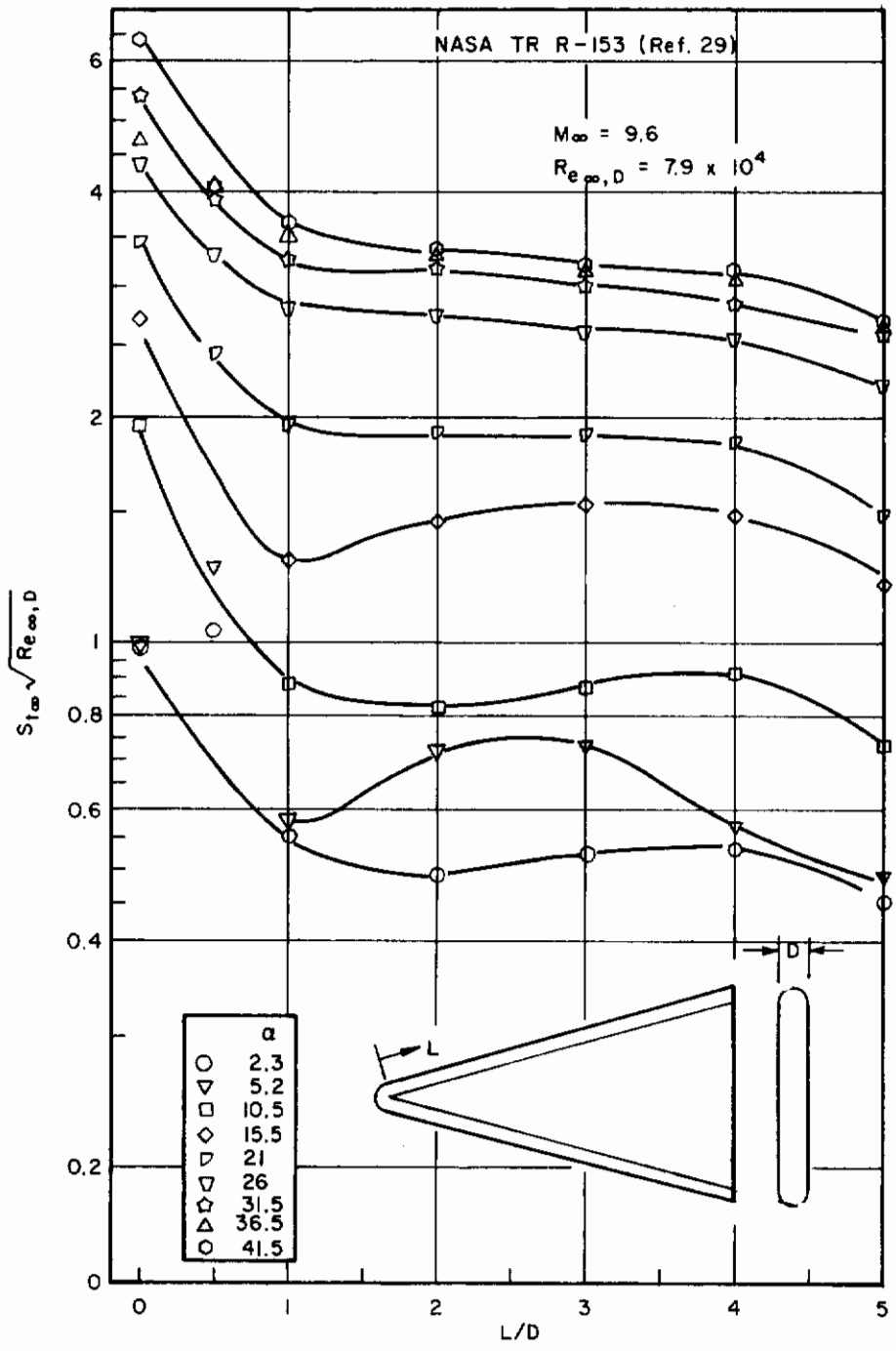

Figure 26. Blunt 70° Delta Wing Tangency Line Heat Transfer Distribution

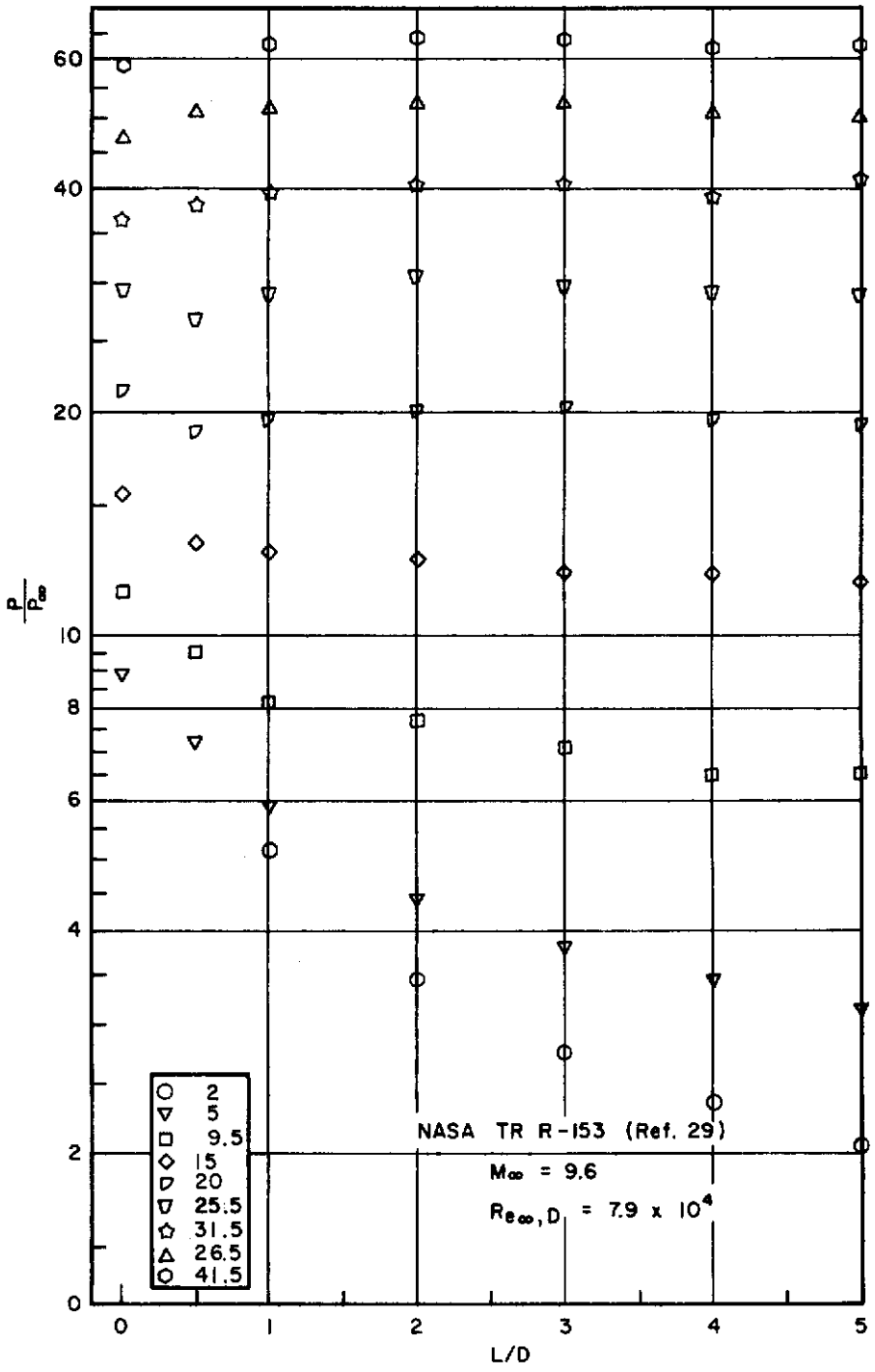

Figure 27. Blunt 70° Delta Wing Tangency Line Pressure Distribution

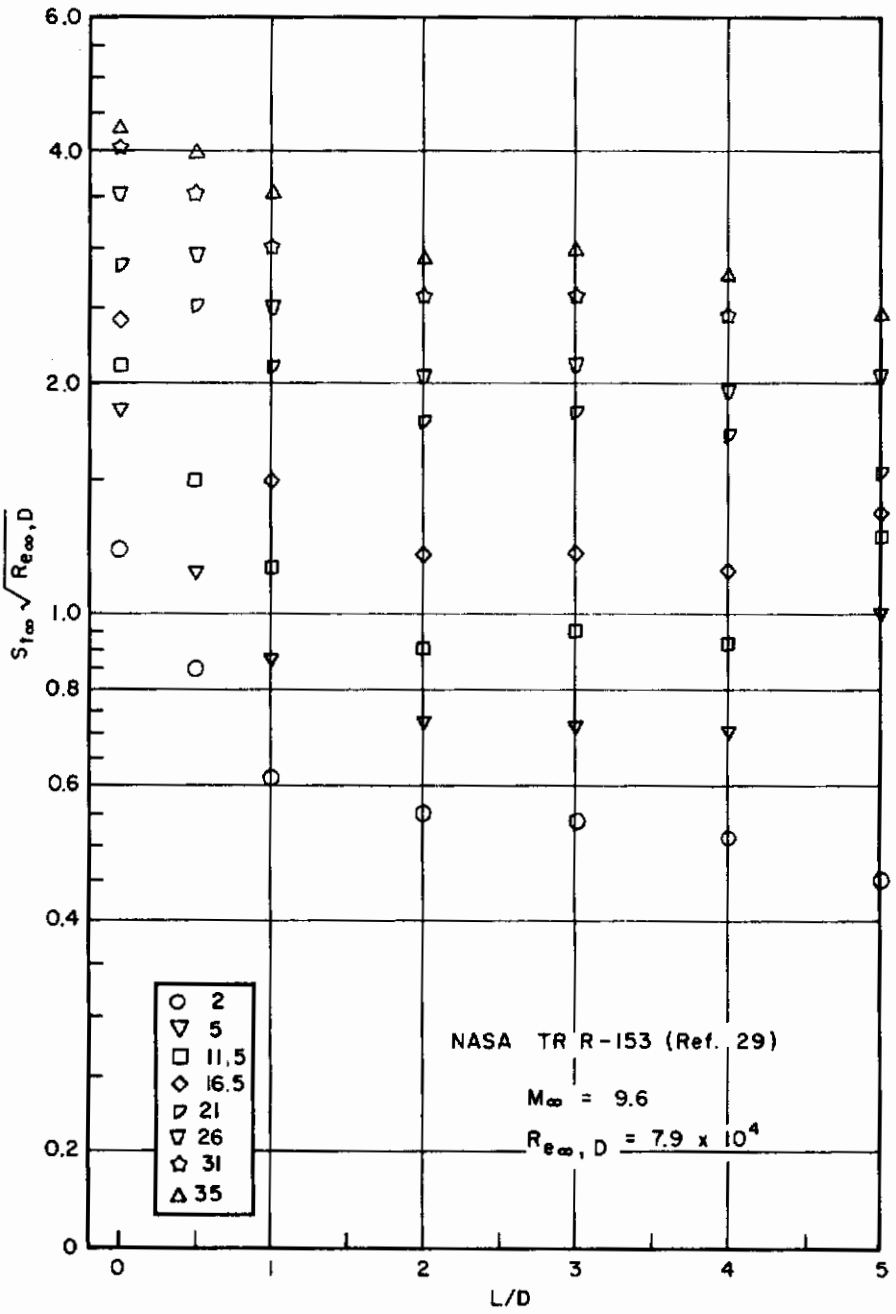

Figure 28. Sharp Nose, 70° Delta Wing Tangency Line Heat Transfer Distribution

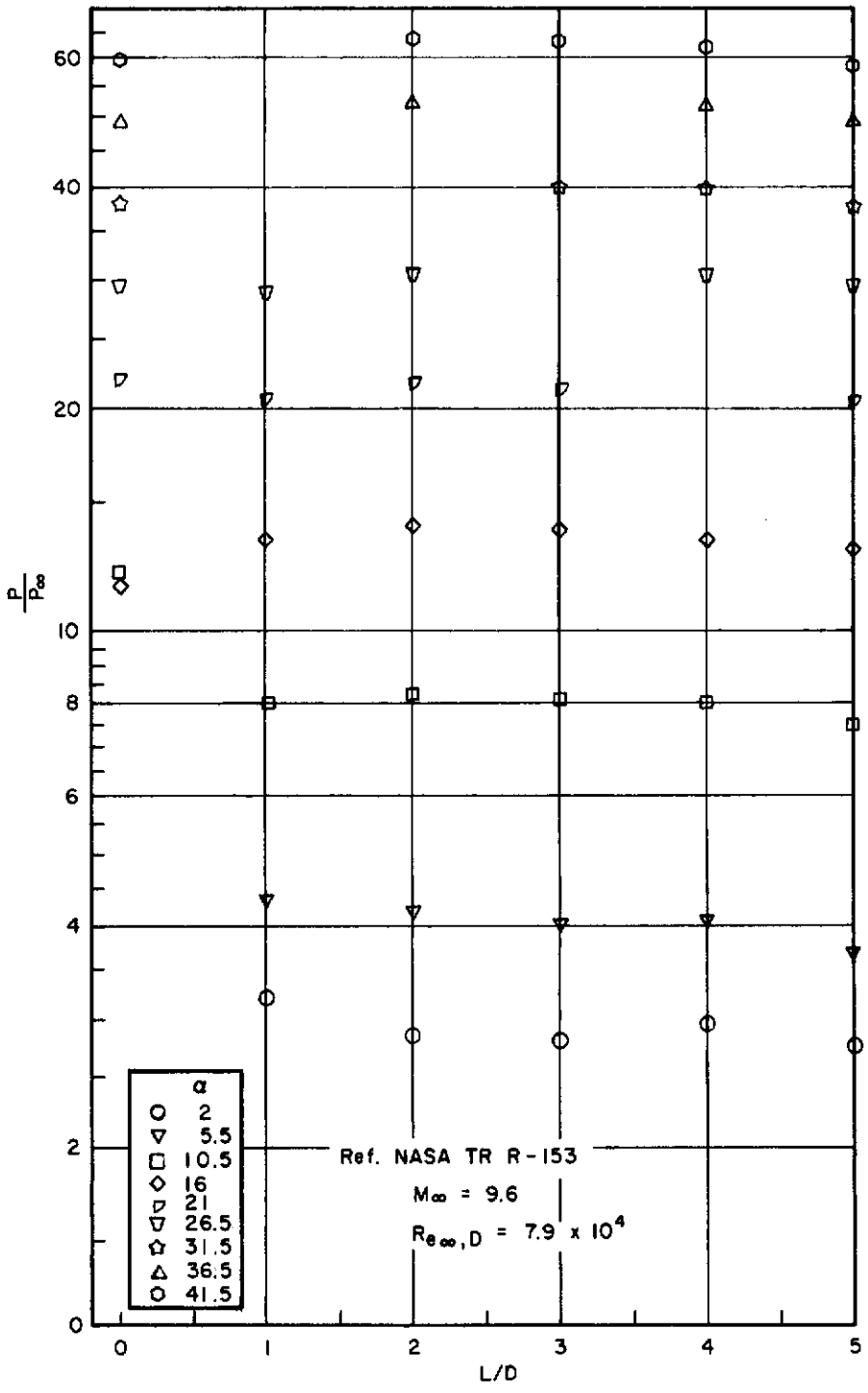

Figure 29. Sharp Nose, 70° Delta Wing Tangency Line Pressure Distribution

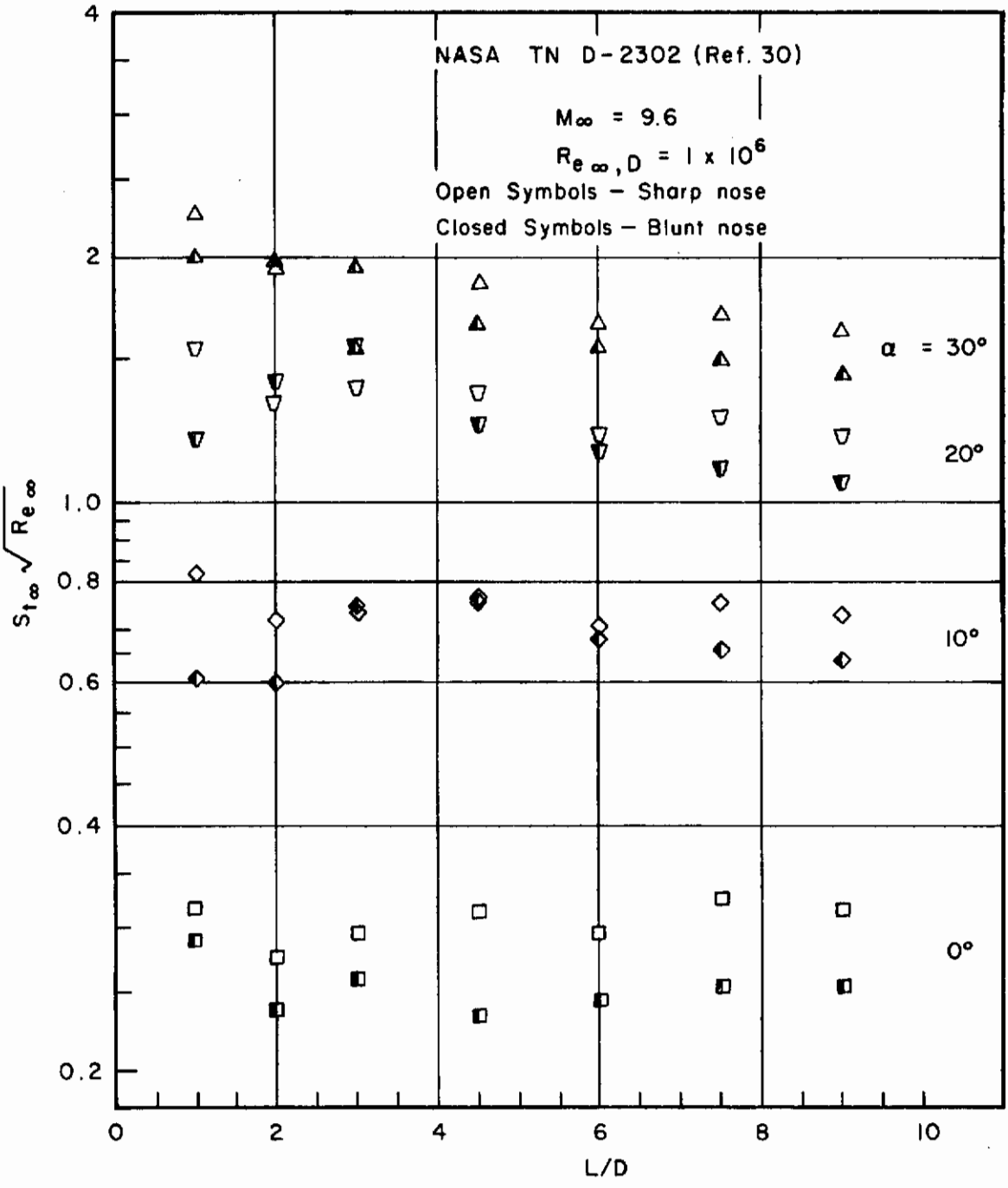

Figure 30. Sharp and Blunt Nose, 70° Delta Wing Tangency Line Heat Transfer Distribution

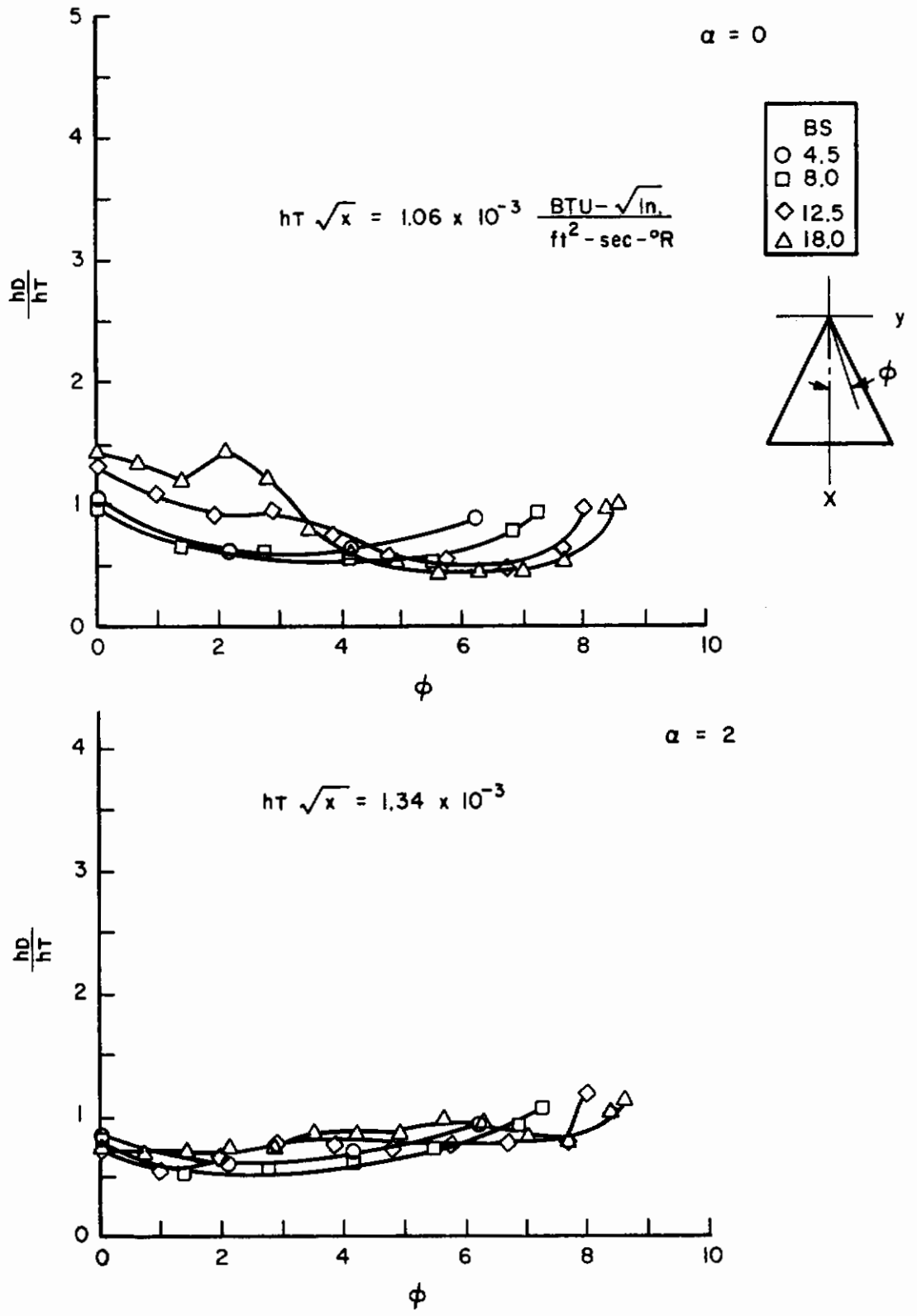

Figure 31. Off Center Line Heat Transfer Distributions on Model 4 at Mach 8, Re /ft = 2 x 10^6

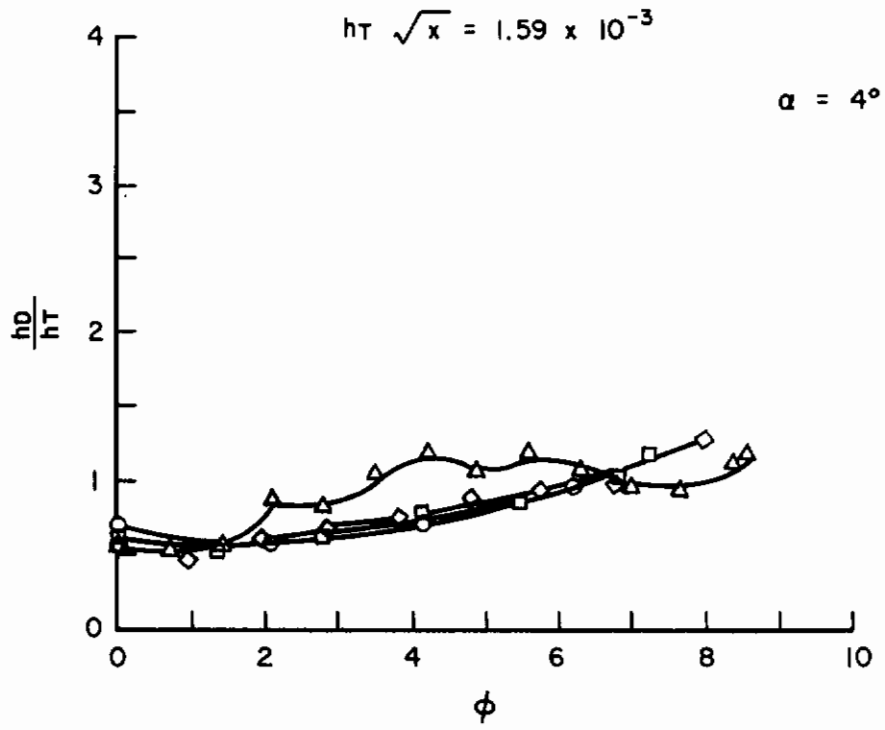

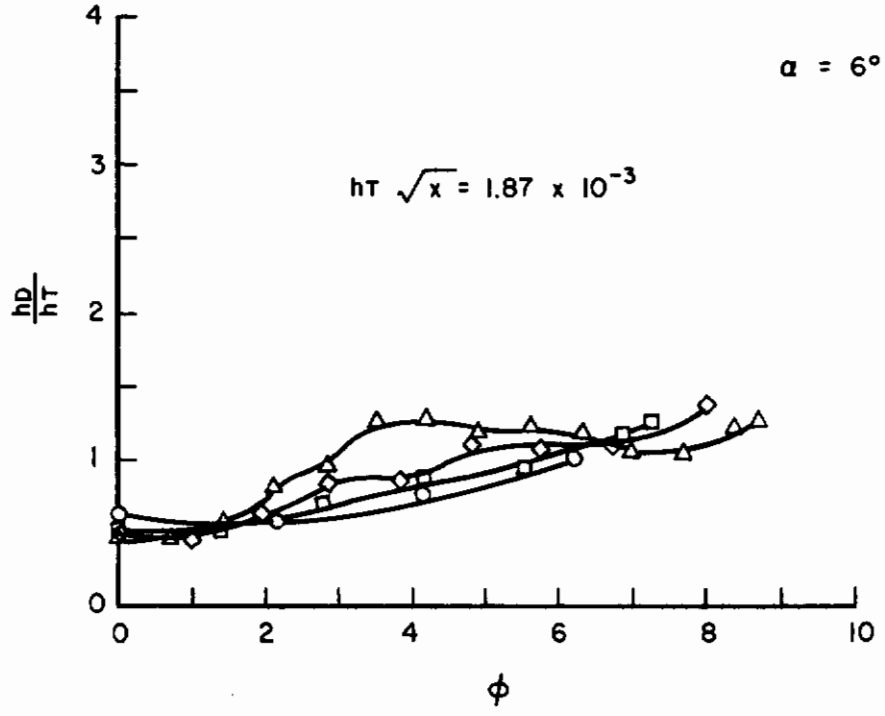

Figure 31 (con't)

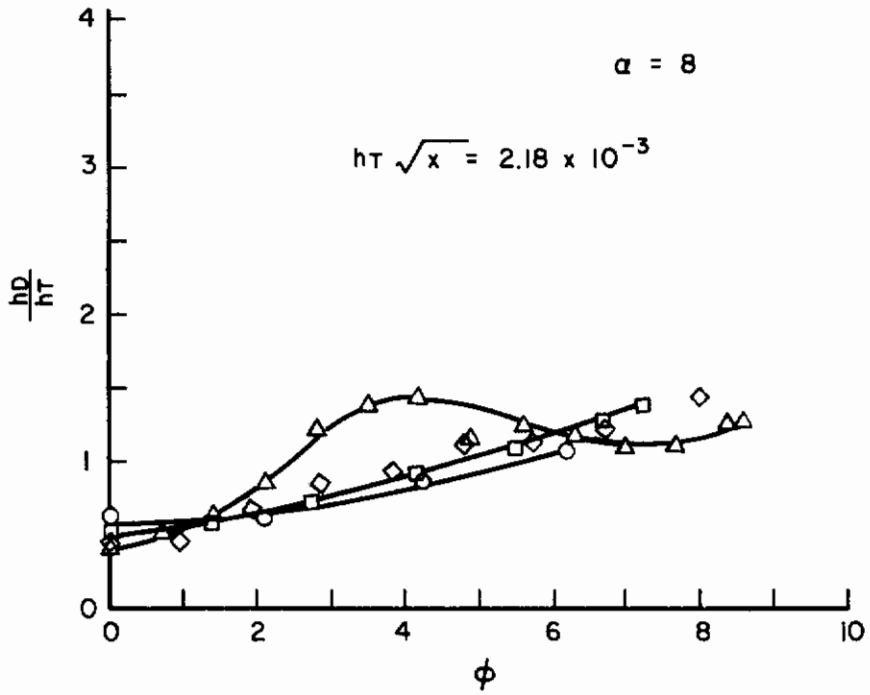

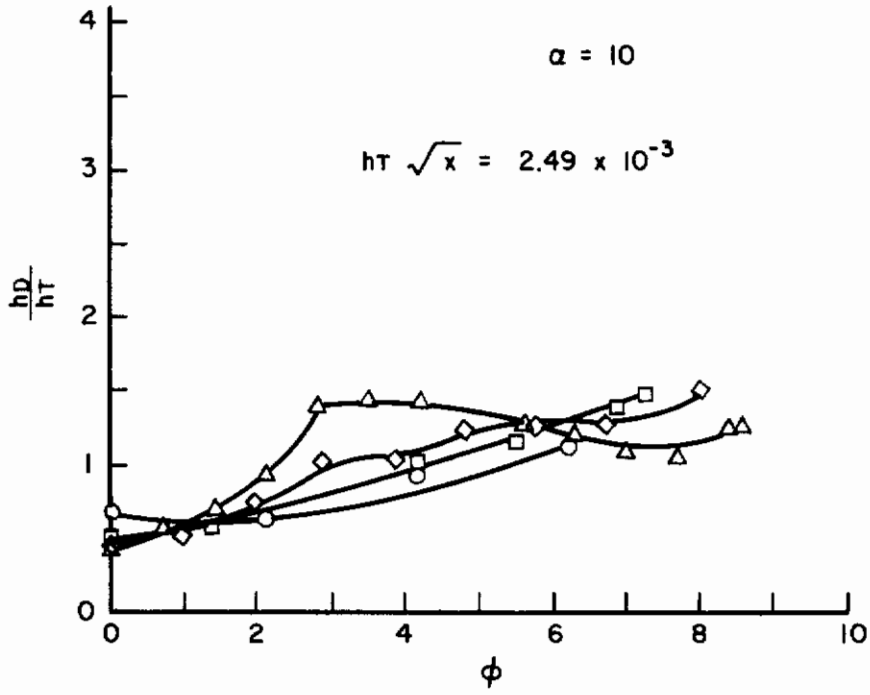

Figure 31 (con't)

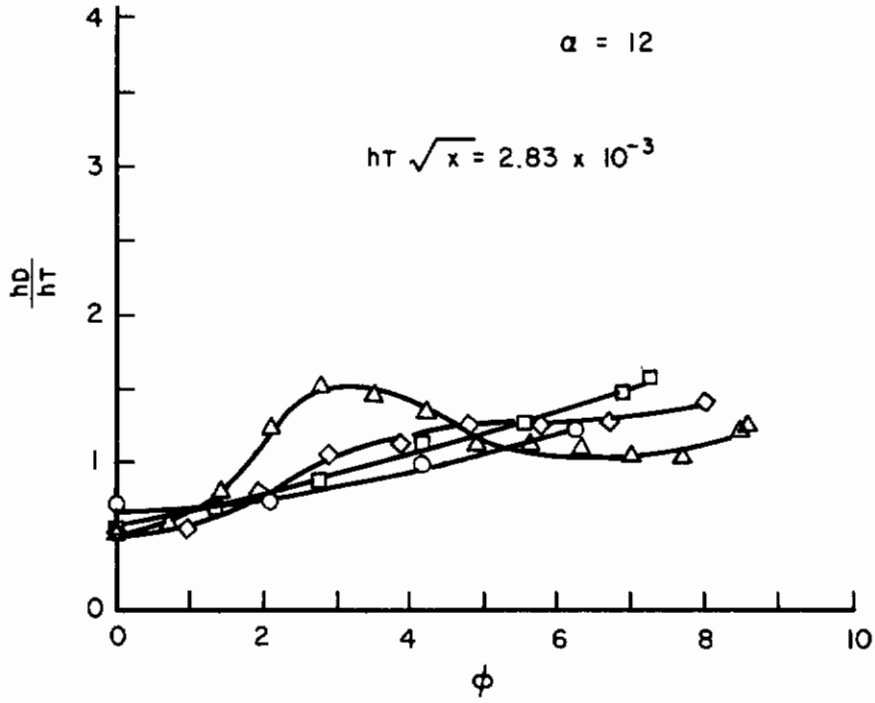

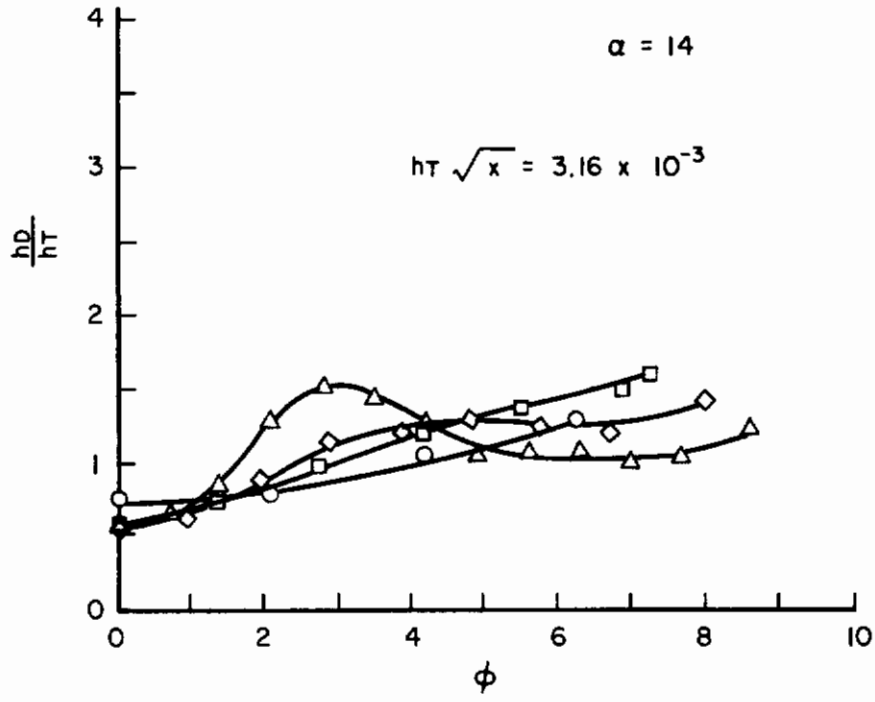

Figure 31 (con't)

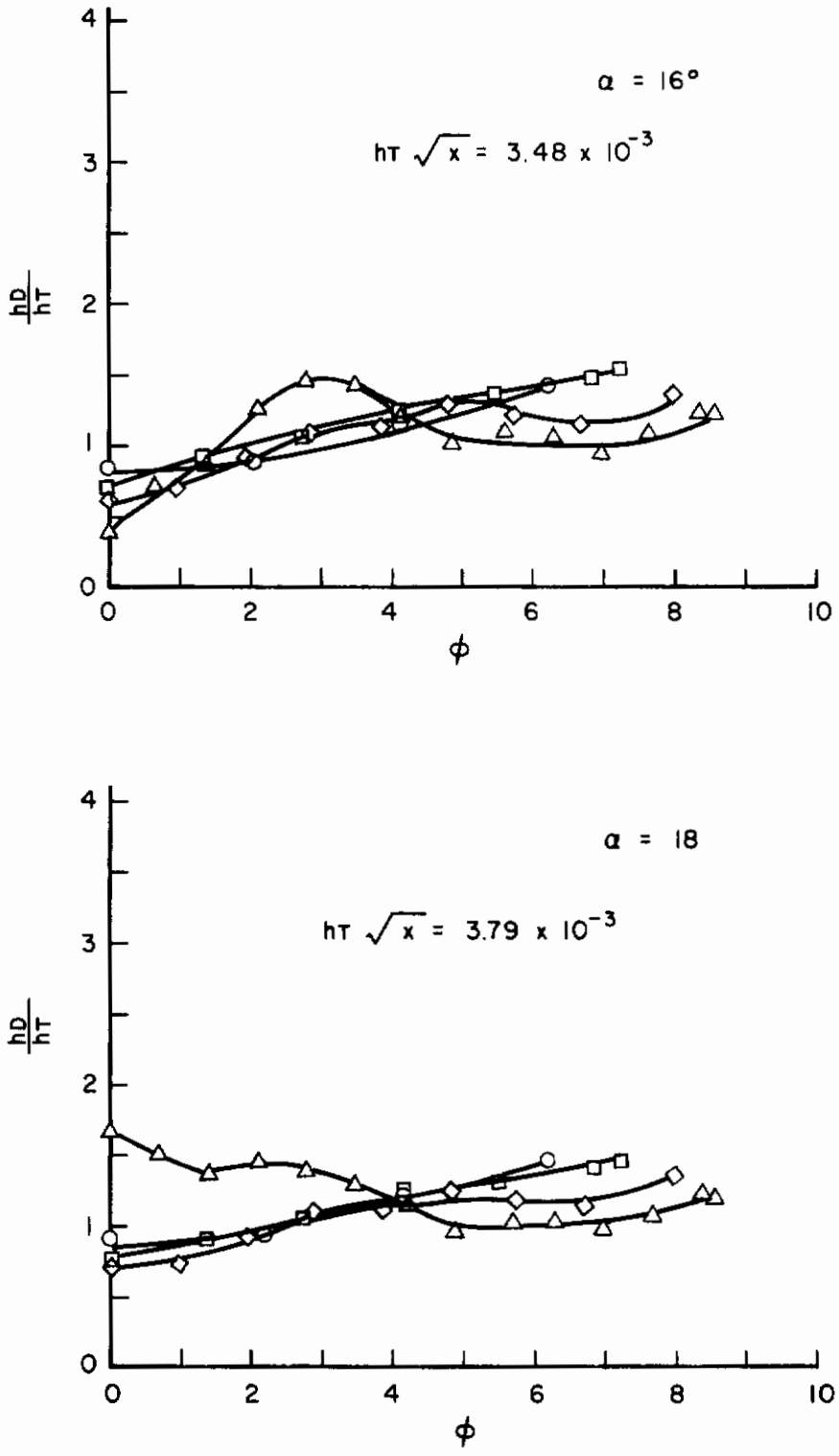

Figure 31 (con't)

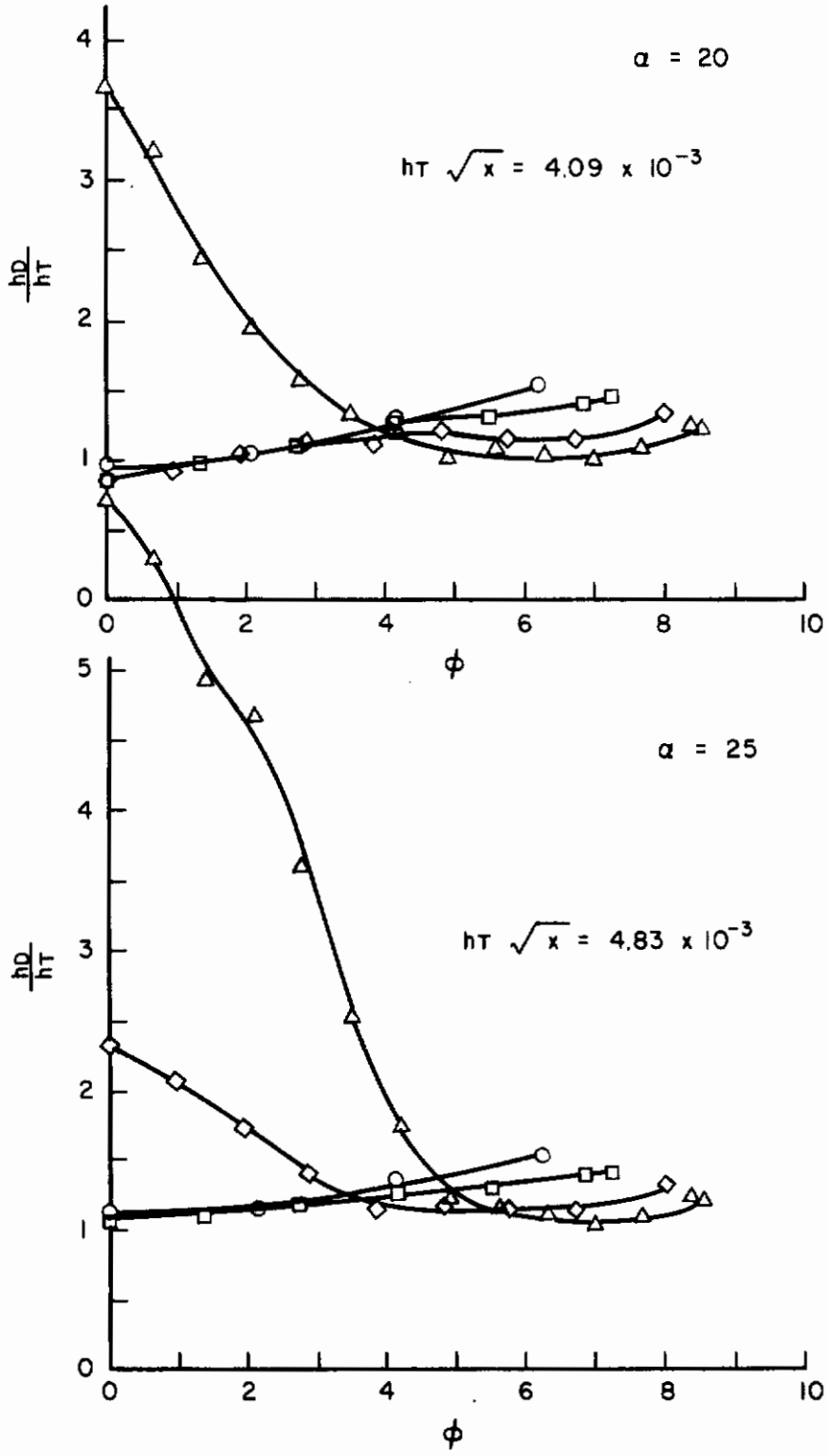

Figure 31 (con't)

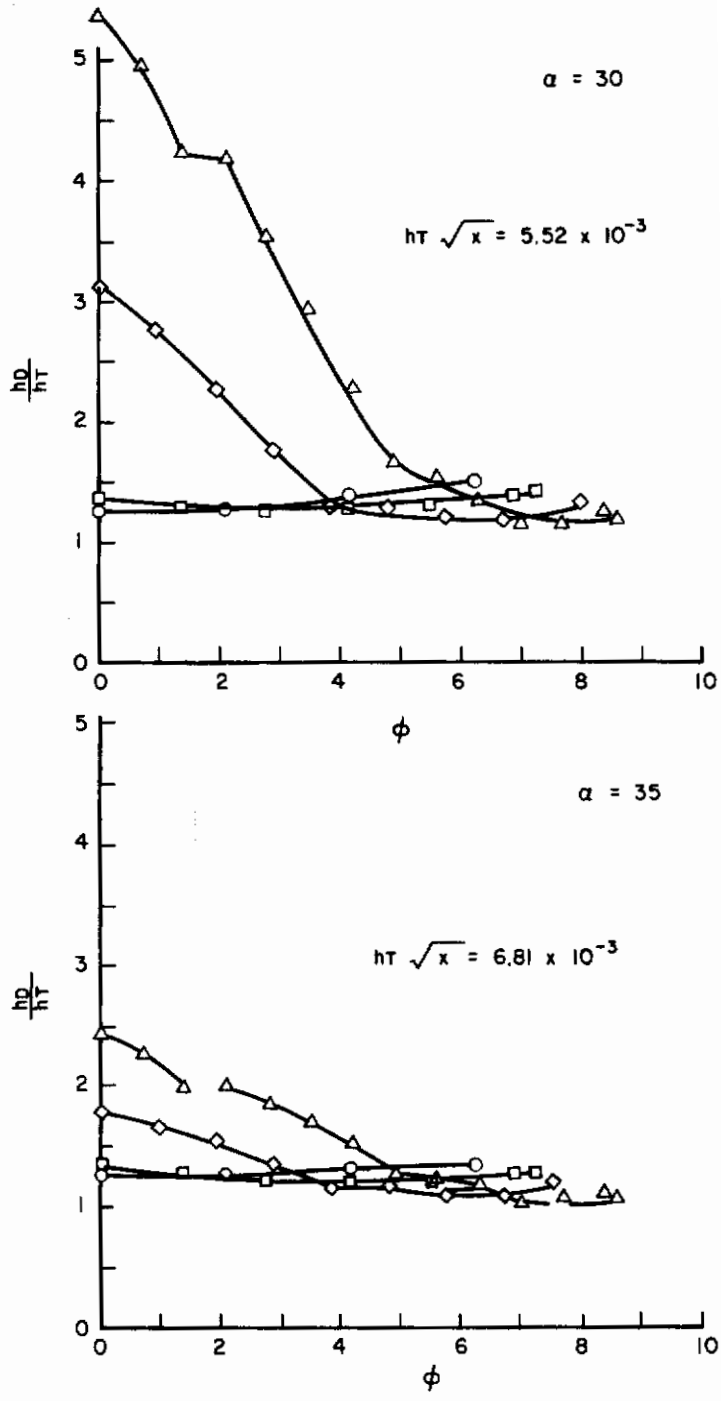

Figure 31 (con't)

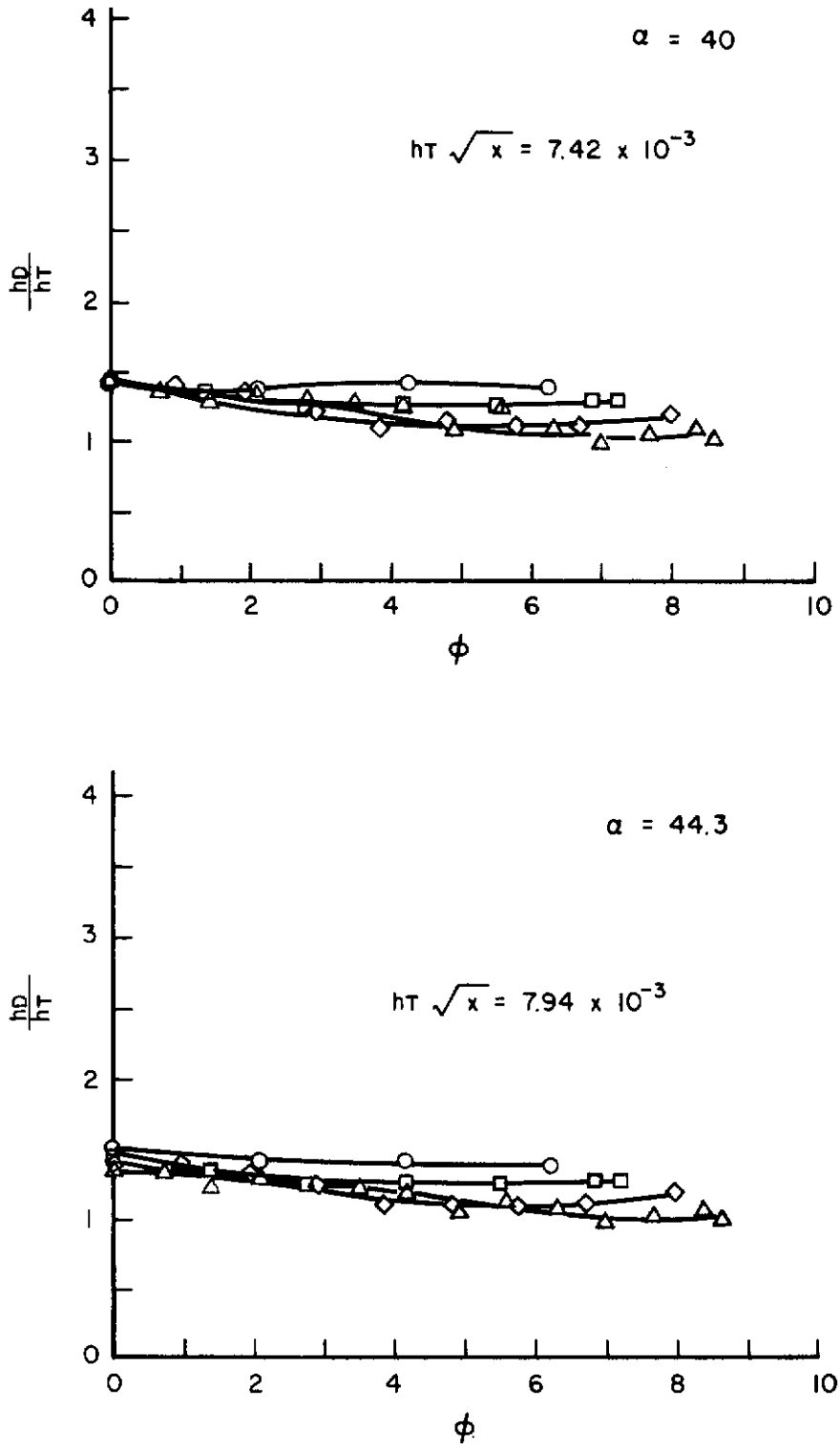

Figure 31 (concluded)

increase at body station 12.5 from α = 10 to 16°. There is an indication of an increase at the near station at α = 18°, but its appearance is nearly masked by transition. The boundary layer is laminar again at angles of attack greater than 40° but there is no evidence of local off-center line increases. Spanwise pressure distributions shown in Figure 32 are seen to be constant.

Results of off-center line heating on the 70° Model 1 are shown in Figure 33. Here the increased heating due to the divergence stream line is seen to be nearer the center line and extend closer to the nose than for the more blunt, higher swept Model 4 and that it moves forward and inward as the angle of attack is increased. The shaded regions in these figures indicate areas of apparently two-dimensional flow in which the heating rate decreases with length as it would on a flat plate. This flow is assumed to have passed through the oblique shock wave which is parallel to the swept leading edge.

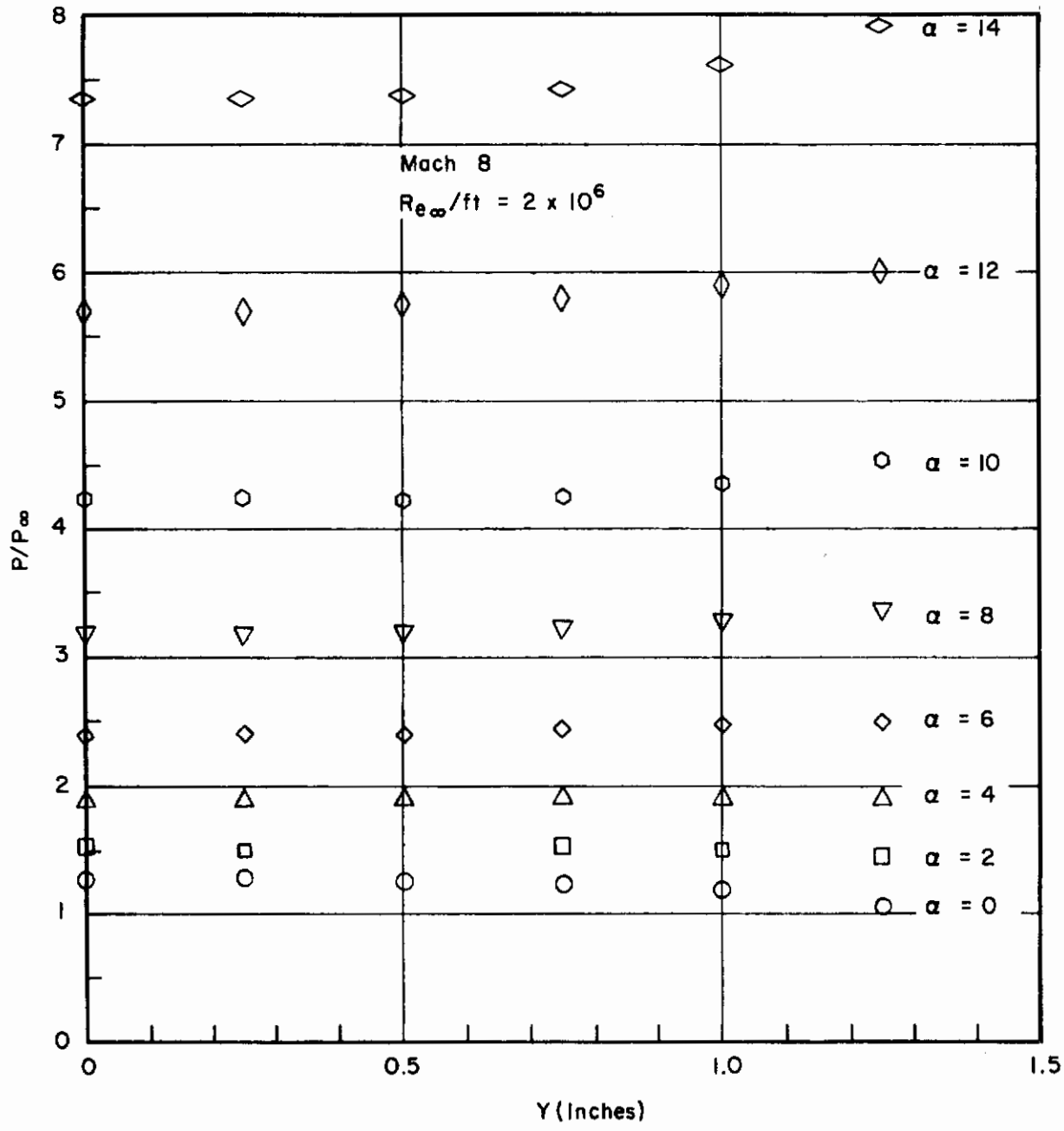

Figure 32a. Off Center Line Surface Pressure Distribution on Model 5 at BS 8

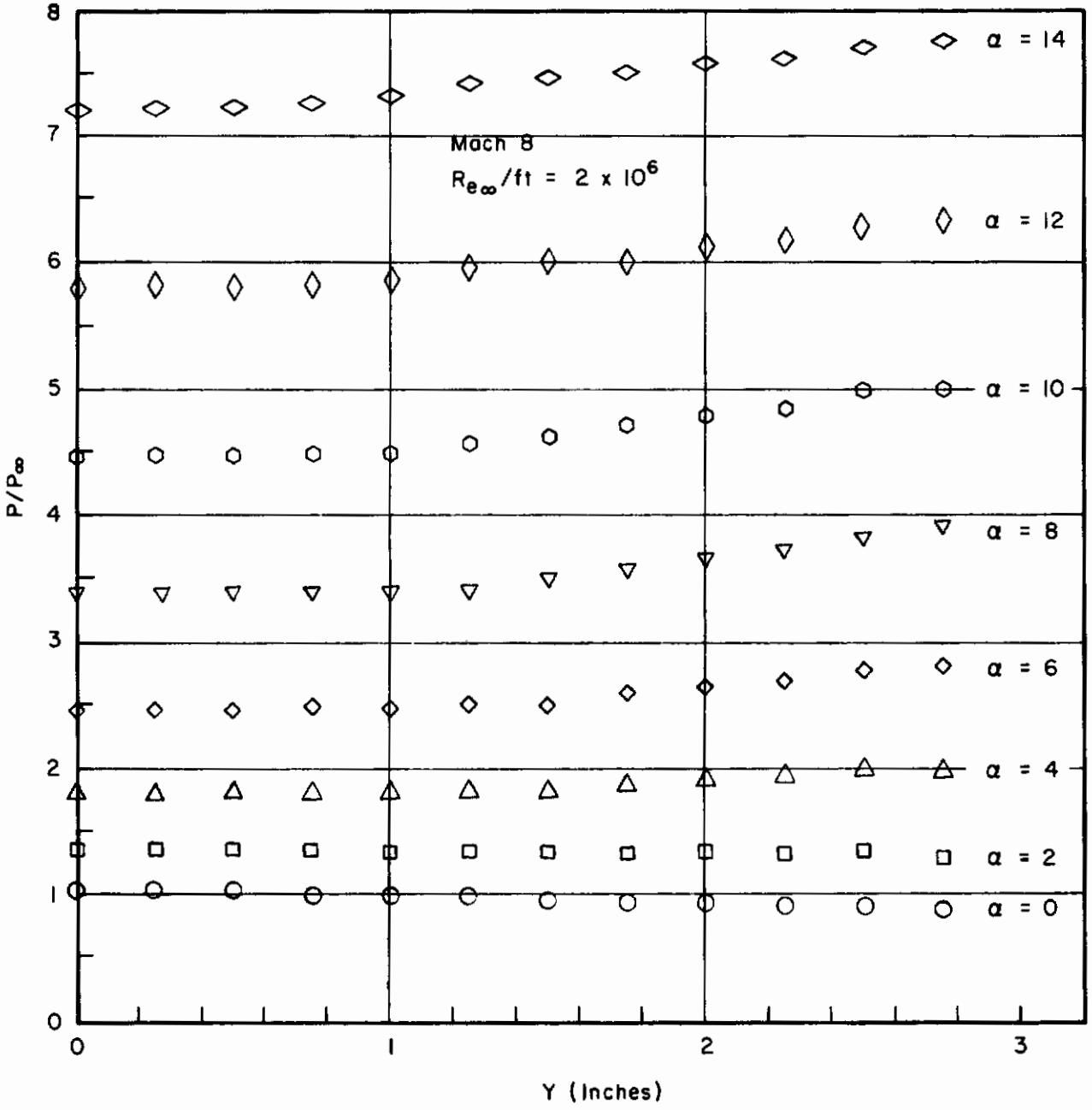

Figure 32b. Off Center Line Surface Pressure Distribution on Model 5 at BS 18

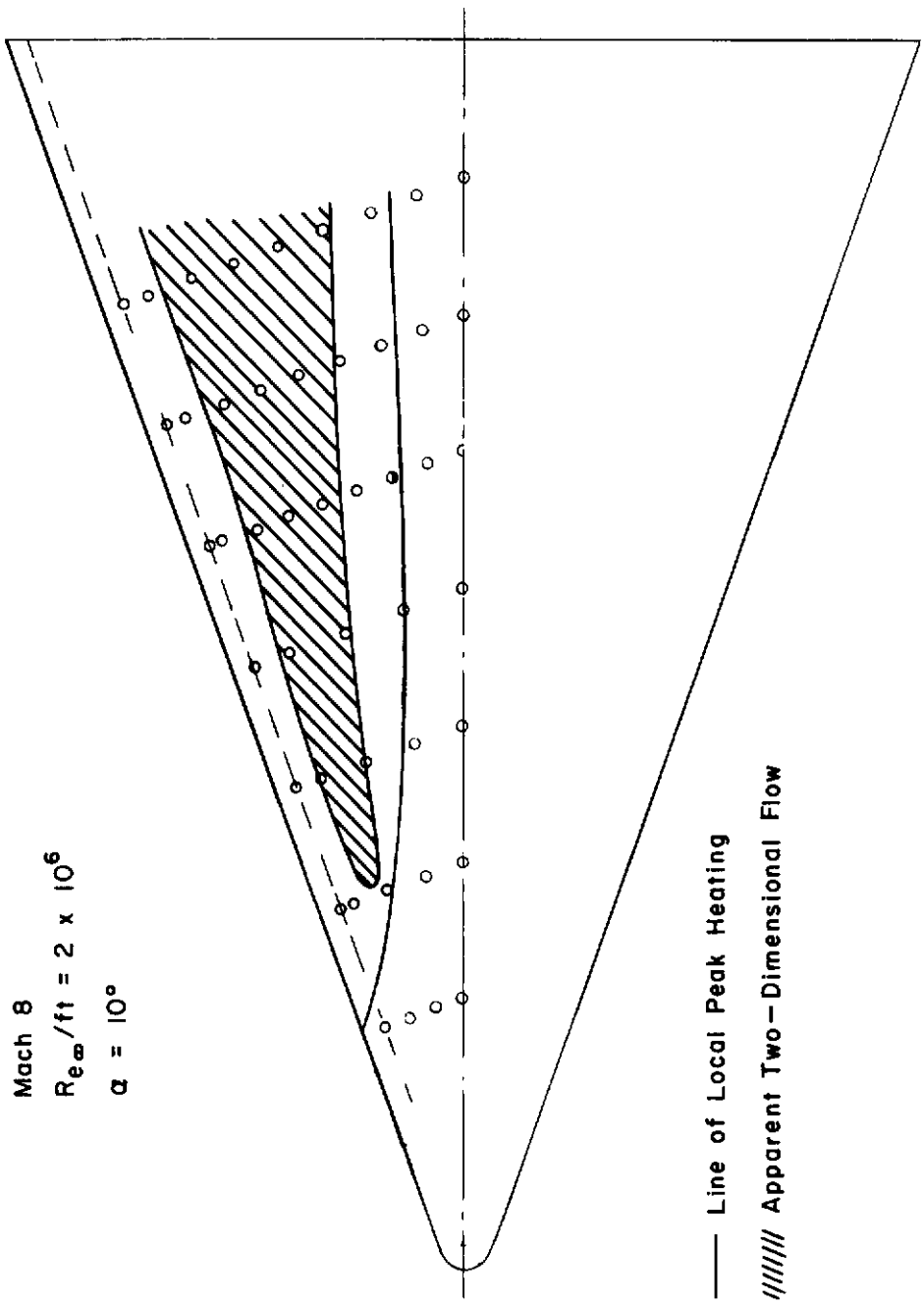

Figure 33. Lower Surface Heat Transfer Patterns on Model 1

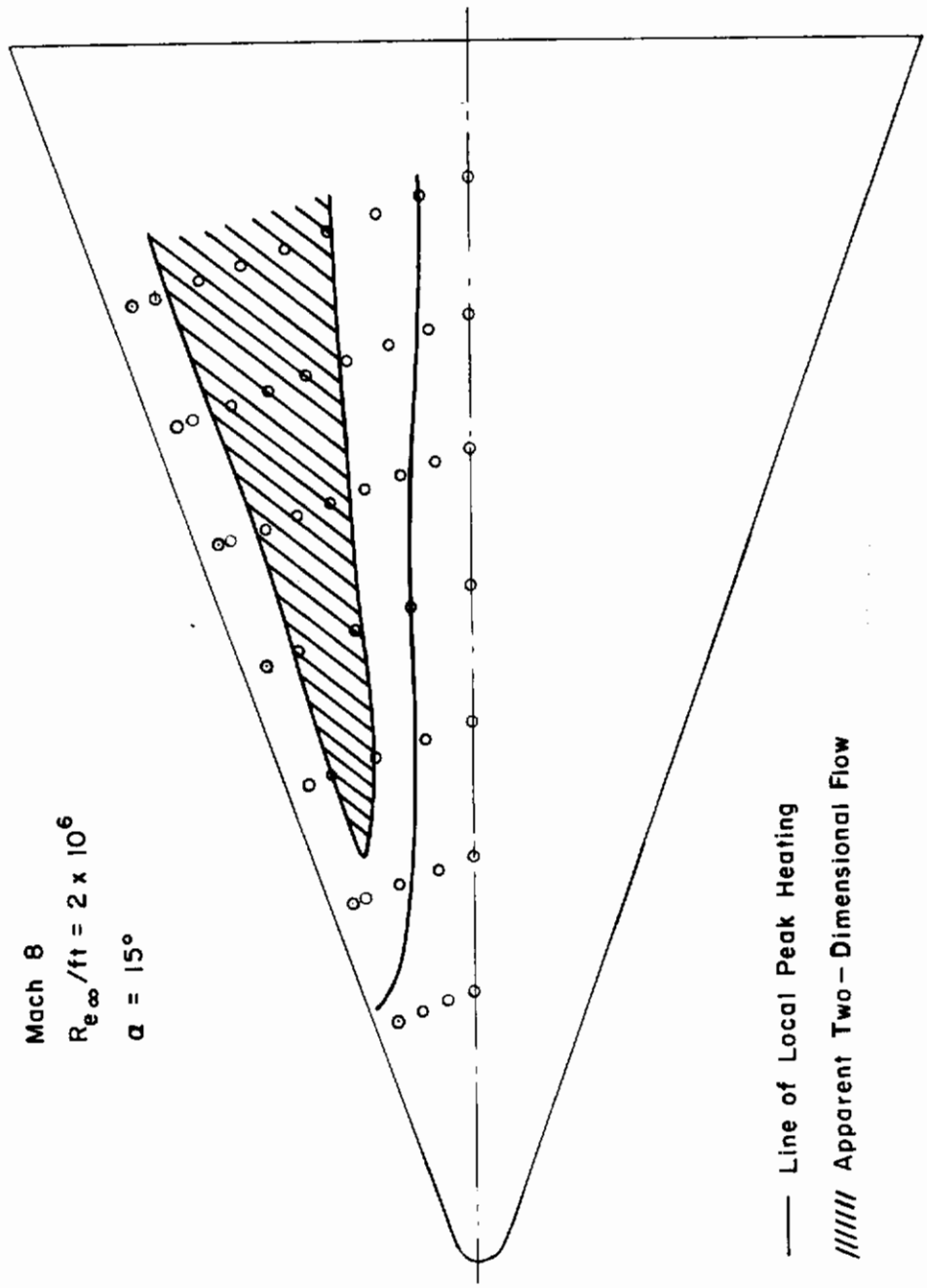

Figure 33 (Con't)

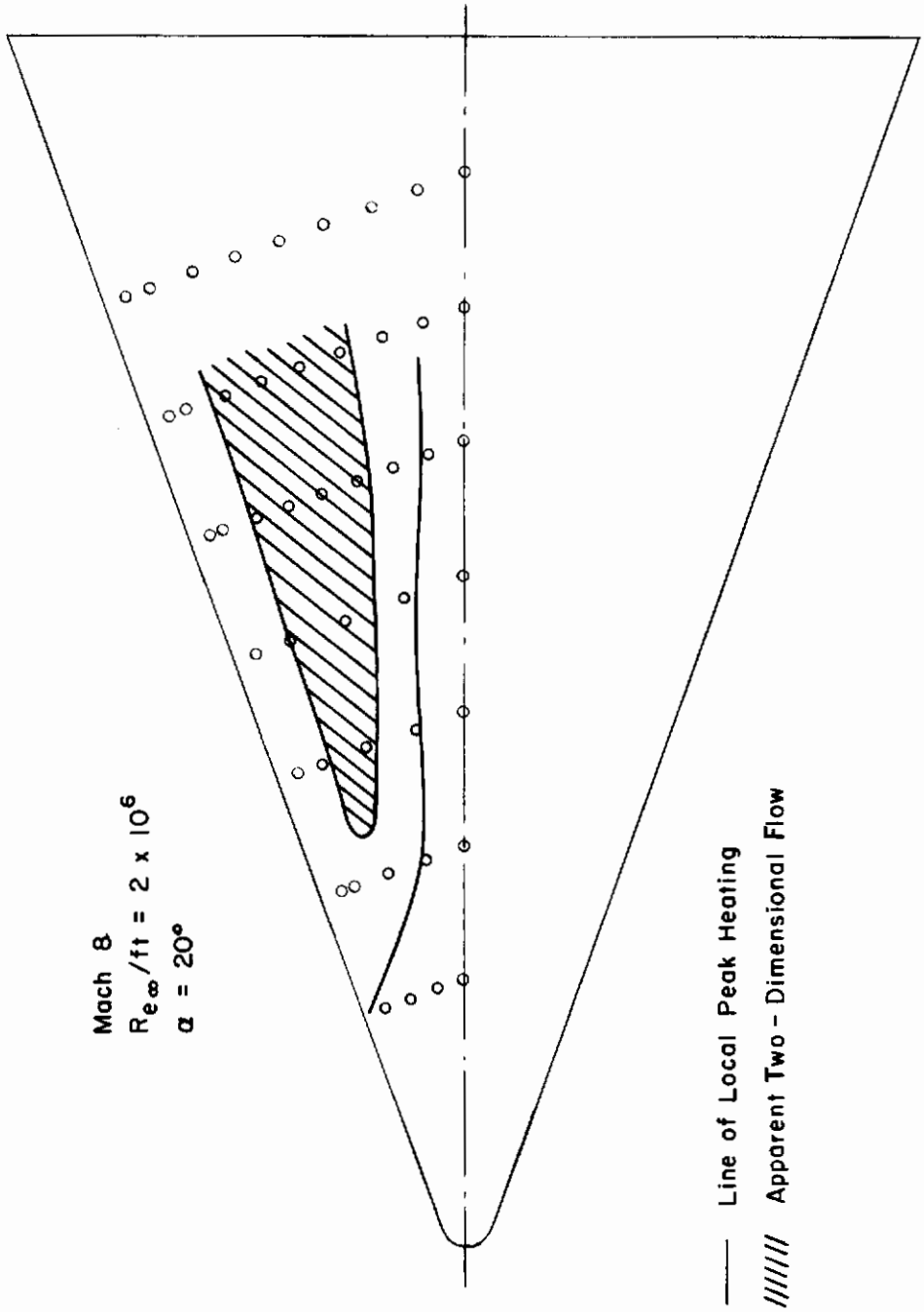

Figure 33 (Con't)

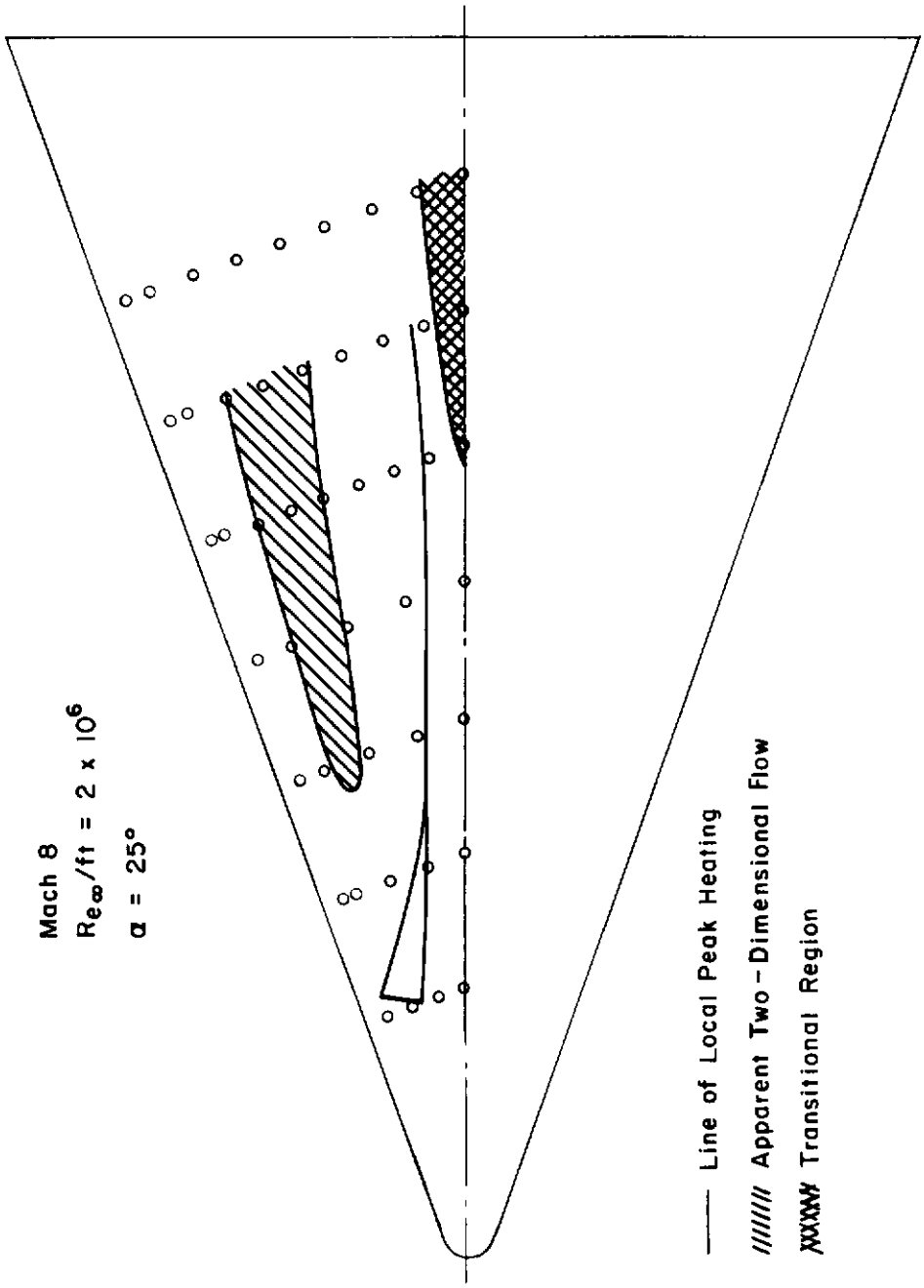

Figure 33 (Con't)

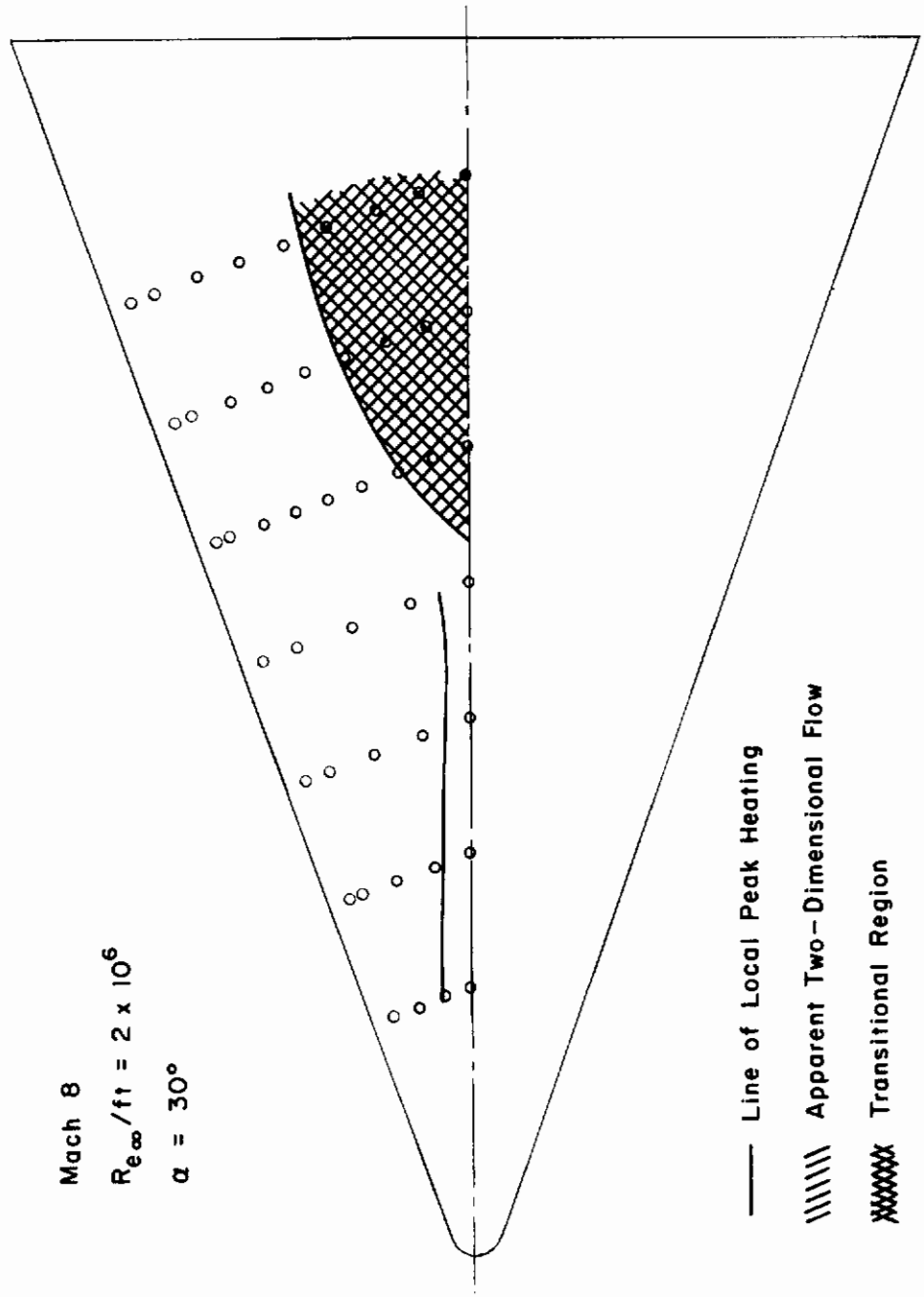

Figure 33 (Concluded)

SECTION IV

RESULTS AND CONCLUSIONS

It can be concluded that there are two different phenomena which affect the flow field on the lower surface of a blunt slab delta wing at angle of attack. One of these determines the extent of blunt nose effects. Pitot pressure surveys taken along a line normal to the center line show the flow near the center line to be in a constant normal shock entropy layer while the flow away from the center line is more indicative of an oblique shock entropy layer. The merging of these two layers can be seen in some of the pitot profiles, especially at Mach 8, $\alpha = 6°$, BS 28 (Figure 16) where it appears that the leading edge flow replaces the normal shock flow next to the model surface.

The origin of the merging line can possibly be traced to an inflection point in the bow shock wave. Planform schlieren photographs in Reference 29 show such an inflection point in the shock shape for blunt nose models which moves forward with increasing angle of attack and a straighter, almost conical shock for a sharp nose model. It is assumed that a slip line is generated between flow with different velocities which has passed through the shock on either side of the inflection point. Therefore, at low angles of attack (α~10°), when the bow shock inflection point occurs farther downstream, the lower surface flow is characterized by the normal shock entropy profile with a constant pitot pressure next to the model surface. As the angle of attack is increased and the inflection point moves forward, more of the lower surface flow is processed by the oblique shock wave downstream of the inflection point and the pitot pressure survey is characterized by the oblique shock profile.

The other phenomena is that the leading edge stagnation line rolls off the leading edge and becomes a divergence stream line on the lower surface. It can be identified and traced through local increases in the heating rate as it crosses the leading edge tangency line and the lower surface.

It was originally thought that these two phenomena were related and that the increased heating on the lower surface was due to vorticity caused by an entropy gradient along the merge line between the leading edge and center line

flow. However, by comparing the location of the merge line in the pitot profiles with that of the increased heating on the lower surface, it appears that the merge line is evident at lower angles of attack and nearer the center line than the divergence stream line and they are not related.

Neither of these effects were seen in the static pressure distribution.

REFERENCES

1. M. H. Bertram, W. V. Feller, and J. C. Dunavant, "Flow Fields, Pressure Distribution, and Heat Transfer for Delta Wings at Hypersonic Speeds" NASA TM X-316, Sept. 1960 (C)

2. J. C. Dunavant, "Investigation of Heat Transfer and Pressure on Highly Swept Flat and Dihedraled Delta Wings at Mach Numbers of 6.8 and 9.6 and Angles of Attack to 90 , NASA TM X-688, June 1962 (C).

3. L. L. Page, P. P. Beardsley, and G. R. Gaumer, "ASSET-Volume IV. Correlative Analysis of Heat Transfer Data," AFFDL-TR-65-31, Vol. IV, Apr. 1966 (C).

4. S. Samet, and J. S. Isenberg, "An Experimental Investigation of Hypersonic Aerodynamic Heating on Highly Swept Delta Wing Configuration", ASD-TDR-62-798, March 1963.

5. A. F. Burke and M. O. Ryder, "Lifting Surfaces in Rarified Hypersonic Flow, Part II: A Blunt, 70 Swept Delta Wing at Angles of Attack", ASD-TDR-62-797, March 1963 AD 299-131.

6. J. E. Wallace and A. F. Burke, "Skin Friction, Heat Transfer, and Pressure Distribution over a Flat Plate and Highly Swept Delta Wings with Sharp and Blunt Leading Edges at Angles of Attack in Hypersonic Flow". ASD-TDR-63-772, Sept. 1963.

7. Stephen W. Rinn, "An Investigation of Heat Transfer on the Asset Vehicle at a Mach Number of 10 and Angle of Attack", AFFDL-TR-65-72, August 1965 (C).

8. M. J. McLaughlin and J. E. Wallace, "Experimental Investigation of Hypersonic, Turbulent Flow and Laminar, Leeward-Side Flow on a 75 Sweep Delta Wing" AFFDL-TR-66-63, Volume II, May 1966 (C).

9. R. T. Savage and C. L. Jaeck, "Investigation of Turbulent Heat Transfer at Hypersonic Speeds, Vol II Analysis of Heat Transfer and Pressure Data on a Flat Plate, Cone, Ogive, Cylindrical Leading Edge, Blunt Delta Wing, and X-15 Aircraft" AFFDL-TR-67-144, Vol II, December 1967 (C).

10. J. E. Wallace, "Applications of the Reference Enthalpy Method for Laminar Skin Friction and Heat Transfer Rates on Delta Wings", AFFDL-TR-69-8, Part II Feb. 1969.

11. J. E. Garberoglio, "Investigation of the Heat Transfer and Pressure Distribution on an 80 Delta Wing-Control Surface Model in Hypersonic Turbulent and Laminar Boundary Layers", AFFDL-TR-69-90, April 1970.

12. E. E. Lindsay, and J. O. Rippey, "Pressure Distribution and Heat Transfer Test on FSL-WADD Delta Wing Configurations at Mach 8 - Phase I", AEDC-TN-60-203, Oct 1960.

REFERENCES (Contd)

13. R. W. Rhudy and R. H. Burt, "Pressure Distribution and Heat Transfer Tests on FSL-ASD Delta Wing Configurations at Mach Number 8 - Phase II, AEDC-TN-61-132, October 1961.

14. A. R. Wallace and E. C. Knox, "Pressure Distribution on Two Hypersonic Glide Vehicle Configurations at Mach Number 19", AEDC-TDR-62-138, July 1962.

15. A. R. Wallace and H. R. Little, "Heat Transfer and Pressure Distribution on Two Delta Wing Configurations at Mach Number 20", AEDC-TDR-63-114, July 1963.

16. R. H. Burt and R. W. Rhudy, "Pressure Distribution Tests on 70-Deg Swept Delta Wing at Angles of Attack from 0 to 90 Deg and Mach Numbers of 8 and 10. AEDC-TDR-64-5, Jan. 1964.

17. F. K. Hube and R. W. Rhudy, "An Experimental Heat Transfer Investigation of a 70-Deg Swept Delta Wing at Mach Numbers of 6, 8 and 10", AEDC-TDR-64-281, Jan. 1965.

18. J. P. Rhudy and J. B. Carman, "Pitot Pressure Survey of the Flow Field of a 70-Deg Swept Blunted Delta Wing at Angle of Attack", AEDC-TR-65-231, November 1965.

19. John L. White Jr., "Pressure and Heat Transfer Distribution on a Blunt 80-Deg Swept Delta Wing at Mach Number 19", AEDC-TR-67-117, June 1967.

20. R. W. Rhudy, "Mach Number 6 and 8 Heat Transfer Tests of Several 80-Deg Swept Delta Wings", AEDC-TR-67-190, Oct. 1967.

21. T. D. Buchanan and J. G. Coble, "Experimental Study of Viscous Interaction on an AFFDL-General Dynamics Configuration at Mach 19", AEDC-TR-68-134, Aug. 1968.

22. T. D. Buchanan, "High Reynolds Number Aerodynamic Test of a Delta Wing Model at Mach Number 12", AEDC-TR-70-24, Mar. 1970.

23. J. P. Rhudy, "Flow Field Investigation on the Windward Surface of Highly Swept Blunted Delta Wings at Moderate Angles of Attack", AEDC-TR-70-46, June 1970.

24. B. J. Griffith, W. S. Norman, and D. E. Boylan, "Hypersonic Heat Transfer Rates on an AFFDL 80-Deg Slightly Blunted Delta Wing", AEDC-TR-70-178, Oct. 1970.

25. R. K. Matthews, and C. R. Cauble, "Aerodynamic Heating Distribution on Three 80-Deg Swept Delta Lifting Bodies at Mach Number 8", AEDC-TR-70-183, Aug. 1970.

REFERENCES (Contd)

26. H. R. Little, "Windward Laminar Heating Rates on Conical Segments at Mach Numbers of 10 and 17", AEDC-TR-70-255, Dec. 1970.

27. Test Facilities Handbook (Eighth Edition), Arnold Engineering Development Center Dec. 1969.

28. Ames Research Staff, "Equations, Tables and Charts for Compressible Flow", NACA TR 1135, 1953.

29. M. H. Bertram and P. E. Everhart, "An Experimental Study of the Pressure and Heat Transfer Distribution on a 70 Sweep Slab Delta Wing in Hypersonic Flow", NASA TR R-153, 1963.

30. P. E. Everhart and J. C. Dunavant, "Heat Transfer Distribution on 70 Swept Slab Delta Wings at a Mach Number of 9.86 and Angles of Attack up to 90 ", NASA TN D-2302, Oct 1964.

UNCLASSIFIED
Security Classification

DOCUMENT CONTROL DATA - R & D

(Security classification of title, body of abstract and indexing annotation must be entered when the overall report is classified)

1. ORIGINATING ACTIVITY *(Corporate author)*
Air Force Flight Dynamics Laboratory
Air Force Systems Command
Wright-Patterson Air Force Base, Ohio 45433

2a. REPORT SECURITY CLASSIFICATION
Unclassified

2b. GROUP

3. REPORT TITLE
A STUDY OF THE BLUNT SLAB DELTA WING AT HYPERSONIC SPEEDS AND ANGLES OF ATTACK

4. DESCRIPTIVE NOTES *(Type of report and inclusive dates)*
August 1964 - September 1969

5. AUTHOR(S) *(First name, middle initial, last name)*
Gerald L. Burke

6. REPORT DATE	7a. TOTAL NO. OF PAGES	7b. NO. OF REFS
June 1972	74	30

8a. CONTRACT OR GRANT NO.	9a. ORIGINATOR'S REPORT NUMBER(S)
b. PROJECT NO. 1366	AFFDL-TR-71-181
c. Task No. 136607	9b. OTHER REPORT NO(S) *(Any other numbers that may be assigned this report)*
d.	

10. DISTRIBUTION STATEMENT Distribution limited to U.S. Government Agencies only; test and evaluation; statement applied December 1971. Other requests for this document must be referred to the Air Force Flight Dynamics Laboratory (AFFDL/FXG), Wright-Patterson AFB, Ohio 45433.

11. SUPPLEMENTARY NOTES

12. SPONSORING MILITARY ACTIVITY
Air Force Flight Dynamics Laboratory (FXG)
Air Force Systems Command
Wright-Patterson Air Force Base, Ohio 45433

13. ABSTRACT

This report presents information obtained during an extensive AFFDL study of the flow field about blunt, slab delta wings. Data taken during the study include surface heat transfer and pressure, pitot surveys, oil flows, schlierens, shadowgraphs, and vapor screens.

The main lesson of the study is the three-dimensionality of the flow field in addition to the documented effects of inflow and outflow. The most unexpected phenomenon was the appearance of a hot streak on the lower surface of the center line. It is proposed that this region of higher heating is due to a slip line originating at the point of inflection in the shock wave between the bow shock and the leading edge shock. This proposition is supported by pitot pressure surveys and surface pressure distributions.

Other qualitative features of the flow field which are presented include the movement of the leading edge stagnation line onto the lower surface. The relative entropy levels of the flow field and the use of vapor screens in hypersonic tunnels.

DD FORM 1 NOV 68 1473

UNCLASSIFIED
Security Classification

14. KEY WORDS	LINK A		LINK B		LINK C	
	ROLE	WT	ROLE	WT	ROLE	WT
Hypersonic Flow						
Blunt Delta Wings						
Three-Dimensional Flow						

*U.S.Government Printing Office: 1972 — 759-484/009